



# Seismic monitoring of torrential and fluvial processes

Arnaud Burtin<sup>1,a</sup>, Niels Hovius<sup>1</sup>, and Jens M. Turowski<sup>1,2</sup>

<sup>1</sup>GeoForschungsZentrum, Helmholtz Centre Potsdam, Potsdam, Germany

<sup>2</sup>Swiss Federal Research Institute WSL, Birmensdorf, Switzerland

<sup>a</sup>now at: Institut de Physique du Globe de Paris, Sorbonne Paris Cité, Université Paris Diderot,  
UMR 7154 CNRS, Paris, France

*Correspondence to:* Arnaud Burtin (burtin@ipgp.fr)

Received: 19 November 2014 – Published in Earth Surf. Dynam. Discuss.: 15 December 2014

Revised: 30 January 2016 – Accepted: 22 February 2016 – Published: 5 April 2016

**Abstract.** In seismology, the signal is usually analysed for earthquake data, but earthquakes represent less than 1 % of continuous recording. The remaining data are considered as seismic noise and were for a long time ignored. Over the past decades, the analysis of seismic noise has constantly increased in popularity, and this has led to the development of new approaches and applications in geophysics. The study of continuous seismic records is now open to other disciplines, like geomorphology. The motion of mass at the Earth's surface generates seismic waves that are recorded by nearby seismometers and can be used to monitor mass transfer throughout the landscape. Surface processes vary in nature, mechanism, magnitude, space and time, and this variability can be observed in the seismic signals. This contribution gives an overview of the development and current opportunities for the seismic monitoring of geomorphic processes. We first describe the common principles of seismic signal monitoring and introduce time–frequency analysis for the purpose of identification and differentiation of surface processes. Second, we present techniques to detect, locate and quantify geomorphic events. Third, we review the diverse layout of seismic arrays and highlight their advantages and limitations for specific processes, like slope or channel activity. Finally, we illustrate all these characteristics with the analysis of seismic data acquired in a small debris-flow catchment where geomorphic events show interactions and feedbacks. Further developments must aim to fully understand the richness of the continuous seismic signals, to better quantify the geomorphic activity and to improve the performance of warning systems. Seismic monitoring may ultimately allow the continuous survey of erosion and transfer of sediments in the landscape on the scales of external forcing.

## 1 Introduction

A multitude of geomorphic processes act on the Earth's surface, driving the evolution of its landscapes. These processes include, for example, river sediment transport, river bed erosion, debris flow, and hillslope activity such as rock fall and landsliding, all of which act at diverse spatio-temporal scales. Moreover, interactions and feedbacks may occur amongst these processes, within individual episodes of geomorphic activity or at longer timescales (Whipple, 2004). For example, a common concept is that hillslopes provide sediment to a river (Hovius et al., 2000), where it serves as a tool for erosion of the channel (Sklar and Dietrich, 2001; Attal and Lavé, 2006; Turowski et al., 2007; Cook et al., 2013).

Channel lowering or lateral undercutting of the banks can in turn drive further erosion of adjacent hillslopes (Densmore et al., 1997; Molnar et al., 2010; Burtin et al., 2014). Such links between separate process domains determine the dynamics of the Earth's surface, and need to be resolved to understand the landscape as a whole. It can be difficult to directly observe geomorphic processes and especially their links, and monitoring techniques often lack the temporal and spatial coverage and resolution to address the scale of interest. Thus, the development of observational approaches that offer continuous coverage of surface process activity at the landscape scale is a key challenge in geomorphology. Not only are such approaches essential to the advancement of understanding of individual processes and landscape dynam-

ics, but they can also be used for natural hazard assessment, real-time event warning (e.g. Berti et al., 2000; Badoux et al., 2009), and monitoring in civil engineering applications. Seismic monitoring techniques are promising in this respect, as the only currently available method to monitor an integral landscape at high temporal resolution, without the need to focus on a specific process or site (Burtin et al., 2013). In the past decades, the potential of using acoustic and seismic signals for geomorphological gain has been explored in several studies (e.g. Bazinger and Burch, 1990; Taniguchi et al., 1992; Govi et al., 1993; Rickenmann and McArdell, 2007; Burtin et al., 2008, 2010, 2011; Gray et al., 2010; Hsu et al., 2011; Schmandt et al., 2013; Díaz et al., 2014; Roth et al., 2014; Chao et al., 2015; Barrière et al., 2015a). The approach makes use of the fact that the displacement of mass at the Earth's surface generates elastic seismic waves that propagate through the subsurface and can be recorded by acoustic or seismic sensors.

A simple particle drop experiment made on a dry gravel-bed channel illustrates the potential of monitoring geomorphic mass movements with seismic sensors and, to a certain extent, the characterization of geomorphic processes (Burtin et al., 2011). Two different rocks with masses of 45 and 0.07 kg weight were dropped from 1 m height, and the induced elastic waves were recorded by a seismometer located at 7 m from the impact. Two immediate observations can be made qualitatively from the recorded signal (Fig. 1): the heavier rock generates a seismic signal with an amplitude 30 times larger than the lighter rock and with a longer wavelength (lower frequency).

Based on this simple experiment, one can expect that a process in which solid matter moves over the surface of the Earth generates seismic waves that carry information about the location, timing and magnitude of that process in their time series and frequency content. Indeed, seismic and acoustic methods are used routinely to monitor geomorphic processes such as snow avalanches (e.g. Suriñach et al., 2000; Bessasson et al., 2007) and bedload transport (e.g. Gray et al., 2010; Rickenmann et al., 2012) and are employed on an operational basis in natural hazard warning systems (e.g. Badoux et al., 2009). Established applications have mainly targeted a specific process at a specific site. Streamside or landscape-wide monitoring concepts are not yet established as a standard tool in geomorphology, but proof-of-concept studies have been described for several processes such as debris flows (Burtin et al., 2009, 2014), bedload transport (Govi et al., 1993; Burtin et al., 2008, 2010, 2011; Hsu et al., 2011; Schmandt et al., 2013; Roth et al., 2014) and rock slides (Helmstetter and Garambois, 2010; Deparis et al., 2008; Dammeier et al., 2011), and path-finding scientific applications have been published (Ekström and Stark, 2013; Burtin et al., 2014).

Here, we review the principles, advantages and current limitations of seismic monitoring of geomorphic processes. First, we introduce some basic concepts of seismology and

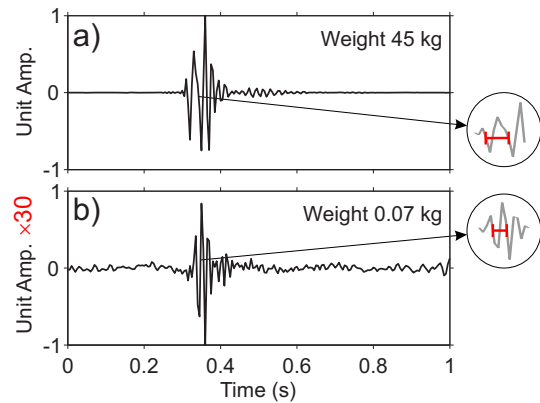


**Figure 1.** Rock drop experiment on a dry gravel-bed channel in the French Alps, Pré de Madame Carle (Burtin et al., 2011). Particles with a weight of 45 kg (a) and 0.07 kg (b) fall from a height of 1 m. The ground vibrations are recorded by a seismometer at a distance of 7 m from the impact. Amplitude is normalized for each drop but the 45 kg particle has a seismic signal 30 times larger than the 0.07 kg one. A longer wavelength is also observed on the seismic signal from the heaviest particle.

survey the different instrumentations for recording seismic waves generated by geomorphic sources. Then, we highlight the advantages and drawbacks of a seismic remote sensing approach, explore the use of seismic instrument arrays to detect, locate and characterize geomorphic activity, and discuss the adaptation of the network geometry to the geomorphic process or process system of interest, illustrating each point with practical examples. Finally, we preview the development of seismic tools for the real-time high-resolution monitoring of Earth's surface processes.

## 2 Seismic monitoring

### 2.1 Signal generation and propagation

When a rock particle hits the ground, the kinetic and potential energy of the impact is partially transferred to the medium as seismic energy and carried by seismic waves that propagate and dissipate from the source point. Seismic waves are classified as body waves that travel through the medium as compressional waves or *P* waves (also primary waves), involving volumetric disturbances, and shear waves or *S* waves (also secondary waves), with only shearing deformation, precluding their propagation in fluids (Fig. 2). Following the analytical expression of Aki and Richards (2002), the displacement  $u$  at a position  $\mathbf{x}$  for a point force  $X_0$  is

$$u(\mathbf{x}, t) = u^N(\mathbf{x}, t) + u^P(\mathbf{x}, t) + u^S(\mathbf{x}, t). \quad (1)$$

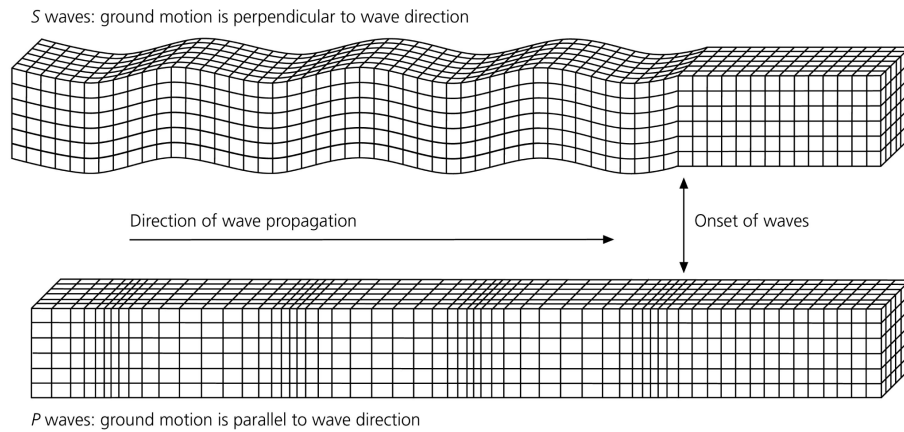


**Figure 2.** Illustration of ground motions produced by compressional (*P* wave) and shear waves (*S* wave). After Stein and Wysession (2003).

In Eq. (1), the ground displacements  $u^P(\mathbf{x}, t)$  and  $u^S(\mathbf{x}, t)$  induced by *P* waves and *S* waves, respectively, are

$$u^P(\mathbf{x}, t) = \frac{A^{FP}}{4\pi\rho\alpha^2} \frac{1}{r} X_0 \left( t - \frac{r}{\alpha} \right), \quad (2)$$

$$u^S(\mathbf{x}, t) = \frac{A^{FS}}{4\pi\rho\beta^2} \frac{1}{r} X_0 \left( t - \frac{r}{\beta} \right). \quad (3)$$

In Eqs. (2) and (3), the point force  $X_0$  is observed at a distance  $r$ , and  $\alpha$  and  $\beta$  are the seismic velocity of *P* and *S* waves, respectively.  $A^{FP}$  and  $A^{FS}$  are radiation patterns changing with respect to the source–receiver position (Aki and Richards, 2002). In these expressions, the ground displacement decays with the travel distance in  $r^{-1}$  because the seismic waves from a source spread in all directions and their amplitude is distributed over an ever-increasing area, which is, to first order, spherical for body waves. Thus, the amplitude per unit area decreases with the distance to the source for body waves. These displacement expressions refer to the far-field terms, because when  $r$  increases, they dominate the near-field term  $u^N(\mathbf{x}, t)$ , which is defined as

$$u^N(\mathbf{x}, t) = \frac{A^N}{4\pi\rho} \frac{1}{r^3} \int_{r/\alpha}^{r/\beta} \tau X_0(t - \tau) d\tau. \quad (4)$$

The amplitude of the near-field decays in  $r^{-3}$  and it dominates the ground displacement when the source–receiver distance is small. The near-field term is composed of both *P* wave and *S* wave motions and the distinction between near- and far-field can be made with respect to the wavelength  $\lambda = c/f$  of the seismic waves propagating with the velocity  $c$  at a frequency  $f$ . The near-field space generally considers an area within less than a small fraction of a wavelength from the source, whereas the far-field space considers an area that is more than several wavelengths (Aki and Richards, 2002).

Seismic waves can also travel along the Earth’s surface as surface waves. These are further subdivided into Rayleigh

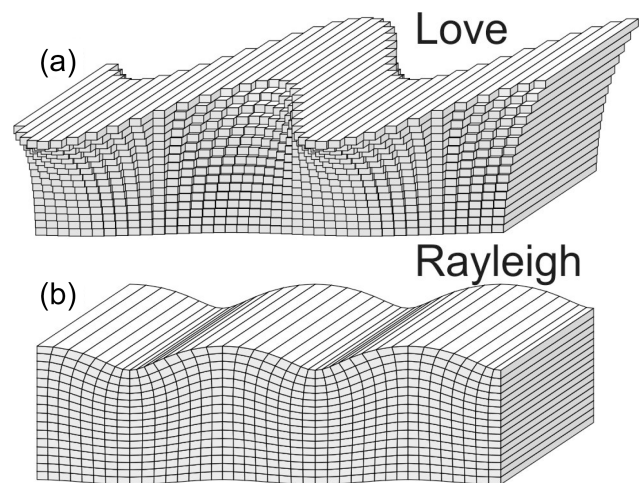


**Figure 3.** Love (a) and Rayleigh (b) surface-wave displacements for a horizontal propagation from left to right. Love waves are purely transverse motion, whereas Rayleigh waves contain both vertical and radial motion. After Shearer (2009).

and Love waves (Fig. 3). Rayleigh waves arise from an interaction between *P* and *S* waves at the free surface and are polarized on the radial and vertical components with a retrograde ellipsoidal particle motion similar to the orbital motion of water under surface waves. Love waves consist of *S* waves polarized in the horizontal plane that are trapped in a wave guide near the surface. Their induced motion is only observed along the transverse direction (Fig. 3). In contrast to body waves, surface-wave energy is distributed over a cylindrical area instead of a sphere. Thus, the amplitude per unit area decreases with the square root of the distance to the source for surface waves. This explains why surface waves have generally the largest amplitude on a seismogram far from the source point.

The seismic energy that radiates from a source is directly linked to the magnitude of the force involved. Forces in-

volved in most geomorphic events are small with dominant frequencies above 1 Hz by comparison with large earthquakes that can excite waves as low as  $\sim 3 \times 10^{-4}$  Hz (e.g. Lay and Wallace, 1995). However, very large landslides also generate seismic waves with frequencies of  $\sim 6 \times 10^{-3}$  Hz (Ekström and Stark, 2013). Seismic energy is dissipated while the wave is travelling, but seismic attenuation is not only due to a geometrical spreading of the energy and it involves other types of dissipation. The energy is also lost by shear heating at grain boundaries or rock mass discontinuities. This attenuation, called anelastic attenuation, is described by a quality factor  $Q_c$ , which is wave-dependent (compressional or shearing) and is inversely proportional to the fractional energy loss per cycle of oscillation (e.g. Lay and Wallace, 1995) as

$$\frac{1}{Q_c} = -\frac{\Delta E}{2\pi E}. \quad (5)$$

Thus, low  $Q_c$  values denote a strongly attenuating medium and we can express the amplitude  $A_0$  as a function of the travel distance  $r$  as

$$A(r) = A_0 e^{-\left(\frac{\pi f}{Q_c v}\right)r}. \quad (6)$$

With this expression, we note that the anelastic attenuation is frequency-dependent and high-frequency seismic waves attenuate more rapidly than low-frequency waves. Indeed, high-frequency waves (short wavelengths) are sensitive to medium heterogeneities with a larger length scale. Low-frequency seismic waves, with long wavelengths, are not affected by these short length-scale heterogeneities that are common at shallow subsurface. Therefore, for low-frequency waves, the medium is seen as a homogeneous body.  $Q_c$  values are also assumed to be frequency-dependent (e.g. Erickson et al., 2004) with a form

$$Q_c = Q_0 (f/f_0)^\gamma. \quad (7)$$

However, for shallow subsurface propagation of a seismic wave,  $\gamma$  can be assumed to be null (Anderson and Hough, 1984).

These developments introduce the role of local ground properties in the way the seismic ground velocity signal  $u(t)$  is recorded. The seismic amplitude can be amplified or altered with respect to a given frequency content. Such behaviours are even more prone to occur with high frequencies, sensitive to small-scale heterogeneities that are dominant in the subsurface. To describe the relevant parameters of the propagating field, one can introduce the Green's function  $G(t)$ , which corresponds to the medium's response to an impulsive force. The Green's function is thus carrying the propagation history from a seismic source at a location  $x_0$  to a receiver at a location  $x$ . Following Aki and Richards (2002) and given a force history  $F(t)$ , the recorded ground velocity  $u(t)$  in the frequency domain is expressed by

$$u(f, x) = 2\pi i f F(f) G(f, x), \quad (8)$$

where  $F(f)$  is the Fourier transform of  $F(t)$ . In the case of seismic sources assimilated to sediment particles in a stream flow, we can assume that forces are vertically incident (Tsai et al., 2012) and Rayleigh surface waves are expected to be the main excited waves (e.g. Sanchez-Sesma et al., 2011). Following this approximation and a Rayleigh-wave sensitivity that decays with depth  $z$  proportional to  $e^{-kz}$ , the amplitude of the Rayleigh-wave Green's function is similar to

$$|G(f, x)| \approx \frac{k}{8\rho_s v_c v_u} \sqrt{\frac{2}{\pi k r}} e^{-\pi f r / (v_u Q)}, \quad (9)$$

where  $\rho_s$  is the volumetric mass density of the medium,  $v_c$  is the Rayleigh-wave phase velocity,  $v_u$  is the group velocity,  $k$  is the angular wavenumber,  $r$  is the source–receiver distance ( $|x - x_0|$ ), and  $Q$  is the quality factor (Tsai et al., 2012). The expression of  $G(t)$  introduces some medium characteristics, like the volumetric mass density, the group velocity and the phase velocity, and the quality factor that are necessary to estimate to properly quantify the seismic amplitude. Therefore, an equivalent source at a similar distance but recorded in a drastically different lithology will imply a different seismic amplitude at receivers. When the quantification of the seismic energy is a key purpose in a study, any observed spatial fluctuation should be compared to local site in order to obtain an integrative picture of the phenomenon.

Ground medium properties are not always well known, but one can state some simple assumptions with respect to the local geology to obtain their estimates. A detailed example of assumptions used in a study case of river seismic noise modelling has been described by Tsai et al. (2012). If a ground exploration is possible, the parameters can be investigated with a common active seismic experiment or even passive seismology using ambient noise correlation (e.g. Shapiro and Campillo, 2004). However, the latter technique has to be carefully applied since the spatial distribution of high-frequency seismic noise does not always allow unbiased velocity estimates. Indeed, homogenous spatial distribution of sources is barely observed at such high frequencies (e.g. Burtin et al., 2010).

Finally, to retrieve the full expressions of the Rayleigh-wave and Love-wave Green's functions, we refer the reader to Aki and Richards (2002) and Tsai and Atiganyanun (2014) for expression relative to surface-to-surface Green's functions as well as Gimbert et al. (2014) for an example of Green's function allowing non-vertical impulsive seismic sources to be taken into account.

## 2.2 Signal recording

Seismic waves or local ground motions are recorded by velocimeters (seismometers or geophones). Accelerometers or strong motion sensors can also be used as seismic instruments. Their use in geomorphic studies is limited since they are less sensitive to small motions than seismometers and we

do not consider them further. Modern seismic instrumentation offers a wide range of sensors with different characteristics that make them suitable for specific applications, like seismic imaging, earthquake monitoring or civil engineering. A key characteristic concerns the frequency response of the instrument or its sensitivity to a given frequency band. Two main instrument categories exist. Short-period seismometers and geophones are sensitive to a high-frequency band, from 1–10 Hz to 500 Hz. These instruments are well suited for the monitoring of most geomorphic sources. The main difference between geophones and short-period seismometers is that the latter is more sensitive to small ground motions, especially at frequencies below 1 Hz. Surface processes also generate low-frequency seismic waves, which require broadband seismometers that commonly have a natural frequency or resonant frequency of the undamped system of  $8.3 \times 10^{-3}$  Hz (120 s period wave). This allows the recording of low-frequency seismic energy induced by large landslides and other mass movements (e.g. Ekström and Stark, 2013). Broadband seismometers are also sensitive to higher frequencies ( $\sim 100$  Hz) but are typically more expensive than short-period seismometers. Therefore, the latter are generally favoured if channel processes are the primary goal. It is important to note that, even if the seismic sensors differ, one can still retrieve an equivalent seismic signal after the removal of the instrument response. Furthermore, the signal deconvolution from the instrument response allows for retrieval of the true motion of the ground (from count to  $\text{m s}^{-1}$ ) and homogenization of observations coming from sensors with different specificities (natural frequency and damping factor). These sensor characteristics influence the true amplitude and phase of the seismic signals. By applying a deconvolution, these artefacts can be corrected. For a complete description, we refer the reader to relevant work on seismometry and reviews (Lay and Wallace, 1995; Aki and Richards, 2002; Shearer, 2009).

Broadband and most short-period seismometers record seismic signals in three dimensions, on orthogonal axes which are commonly aligned vertically, northerly and easterly so that directional information from multiple stations can be compared. The use of three-component instruments allows a larger diversity of data processing than a single-component instrument. For example, the polarity of seismic waves can be used to determine the source type, and it can also give some information about the incoming direction of a wave front in a location problem. Moreover, the analysis of three-component seismic data allows the estimation of possible site effects, which amplify the seismic wave amplitude at a certain frequency due to a specific lithology and/or geometry of sedimentary layers in the medium below the stations. There are diverse strategies to estimate these effects, but the best known approach is the  $H/V$  ratio method from Nakamura (1989), which is largely used in seismic engineering. The approach consists of estimating the spectral ratio of the

seismic energy of the vertical to the horizontal components to highlight the possible amplified frequencies in the signal.

Seismometers are sensitive to small ground motions, corresponding to velocities smaller than  $1 \mu\text{m s}^{-1}$  at a quiet site. They can, but do not have to be, deployed in the immediate vicinity of the studied processes. Crucially, they can also be located at safe sites, removed from geomorphic process activity, where their functioning is not compromised. Their location can be tailored to the monitoring objective, which typically falls into one of two categories. Monitoring is either targeted at a specific process and site or aimed at the use of the ambient seismic noise to study multiple processes interacting over a distributed area. We will discuss these two general classes in the following sections, using the monitoring of bedload transport as an example, as both local and ambient approaches have been used to study this process.

### 2.3 Local monitoring

Geophones are used in several indirect methodologies to survey channelized geomorphic processes such as bedload transport (e.g. Gray et al., 2010) and debris flows (e.g. Comiti et al., 2014). The term indirect indicates that the seismic signal gives direct information only on relative rates, and has to be calibrated to obtain absolute quantities (e.g. Mizuyama et al., 2010a). For in-stream monitoring, geophones are often coupled to steel plates or pipes (e.g. Rickenmann and Fritschi, 2010; Mizuyama et al., 2010b). In such a setup, the sensor records the signal of the impact of sediment particles on the steel casing whilst being protected from the sediment-laden flow. As an additional benefit, it is to some extent possible to isolate the sensor system from noise sources originating outside the channel, and thereby from processes that are not of interest for the application at hand.

Currently, the most advanced in-stream indirect monitoring method for bedload transport is the Swiss plate-type geophone system (Rickenmann et al., 2014; Turowski et al., 2009, 2013) that is used as an example here. Versions of this sensor system have been employed for more than 25 years in the Erlenbach, a small headwater catchment ( $0.7 \text{ km}^2$ ) in the Swiss pre-Alps (e.g. Rickenmann et al., 2012). The stream is instrumented with six geophone plates located in a cross section just upstream of the retention basin. The sensors record the seismic signal of bedload impacting on the plates, and when the amplitude exceeds a pre-defined threshold, an impulse is counted. These impulse counts provide a memory-saving summary statistic that has been proven to be a robust predictor of transported particle mass both in laboratory experiments and in comparison to direct field measurements at the Erlenbach (Fig. 4) and at other sites (Rickenmann and McArdell, 2007; Rickenmann et al., 2012, 2014). A similar technique is used for the Japanese pipe hydrophone and yields comparable results (Mizuyama et al., 2010a, b). Recently developed protocols allow the extraction of the size distribution of the transported grains (Wyss et al., 2014) and

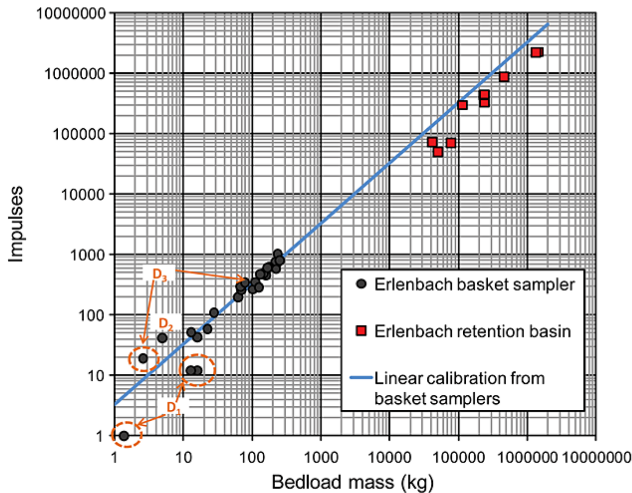


**Figure 4.** Comparison of calibration measurements of geophones and sediment transport from basket samplers (dots) and retention basin (squares) in the in the Erlenbach, Switzerland. After Rickemann et al. (2012). Group data labelled  $D_1$ ,  $D_2$ , and  $D_3$  denote less reliable data (outliers) for the geophone calibration (see Rickemann et al., 2012).

the energy they deliver to the bed (Turowski et al., 2013, 2015).

Local monitoring has distinct advantages and disadvantages over ambient monitoring approaches. Although the initial installation of instrumentation such as the Swiss plate-type geophone system is costly and relies on the existence of a fixed channel cross section such as a check dam, afterwards the sensors are largely maintenance-free and can record at a high temporal resolution for decades. Moreover, the sensor housing is acoustically isolated and only relevant in-stream signals are recorded. Many other types of sensors exist (see Gray et al., 2010), some less sophisticated than the Swiss plate-type geophone system and therefore quicker to deploy, but less stable and more sensitive to noise. Local monitoring solutions provide observations and quantifications of a process at a point. For them to be meaningful, process occurrences must be focused in the location of observation. This is the case for channel processes such as bedload transport and debris flow, but not for other surface processes. If broader spatial coverage is desired, then ambient monitoring is the approach of choice.

#### 2.4 Ambient monitoring

Ambient monitoring has two principle advantages. First, the instruments are installed outside of geomorphically active areas such as channel beds, and are thus easily accessible for maintenance and data collection, and protected from the destructive forces acting during geomorphic events. Second, the instruments are likely to record signals from a variety of processes and distributed sources.

Govi et al. (1993) were the first to explore a stream-side approach for the monitoring of in-channel processes, using six short-period seismometers deployed along a 150 m long coarse-grained alluvial channel in the Italian Alps. These authors analysed the average seismic amplitude from several flood events and highlighted the potential for bedload monitoring. Time–frequency analysis of continuous seismic signals from a temporary seismological experiment deployed across the Himalayas (Hi-CLIMB experiment; Nábělek et al., 2009) showed the importance of the nearby trans-Himalayan Trisuli River in generating the recorded seismic energy (Burtin et al., 2008). The stations along and within 2 km of the Trisuli River displayed an increase in seismic energy between 1 and 20 Hz during the summer monsoon season (Fig. 5). Along the Himalayan Arc, this period shows a drastic increase in water discharge and sediment transport, due to rainfall and melting of Himalayan snow and glaciers (e.g. Barros and Lang, 2003). The relation between high-frequency seismic energy and hydrological parameters (water level and discharge) traces a hysteresis loop (Fig. 5b) with a larger seismic energy during the onset of the monsoon than at the end of the summer at a given water level (Burtin et al., 2008). This indicates that the flowing water is not the only source of river seismic signals and secondary signals are produced by sources in the river, probably moving bedload particles. No bedload data are available for Himalayan rivers at the time of writing, but a similar hysteresis loop between suspended sediment load and water discharge is known from other trans-Himalayan rivers (Gabet et al., 2008; Andermann et al., 2012; Struck et al., 2015), lending some weight to this interpretation. Hsu et al. (2011) also found a hysteresis loop between discharge and seismic noise at the shorter timescale of a typhoon-induced flood along the Cho-Shui River, Taiwan. Roth et al. (2014) confirmed a direct link between the observation of a hysteresis and the occurrence of bedload transport. Using the seismic data recorded along the Chijiawan River in Taiwan after the removal of a check dam, they had the opportunity to record two main storms, for which only one had an episode of bedload transport. A hysteresis between seismic noise and water level was only observed when bedload was mobilized.

To better use the river seismic signals in geomorphology, Tsai et al. (2012) proposed a model for the power spectrum density of seismic waves generated by impulsive impacts from saltating particles. This first attempt to quantify sediment flux from seismic recordings was tested with the data acquired along the Trisuli River (Fig. 5). With a simple sediment transport model (vertical impacts) and some assumptions on the river hydrodynamics, the river grain size distribution and ground seismic properties, the authors were able to reproduce the observed hysteresis and calculate the bedload flux (Fig. 6); however, they did not have bedload transport observations for direct validation. Nevertheless, Tsai et al. (2012) thus developed a first-order direct model to simulate seismic data that can, at least in principle, be used in

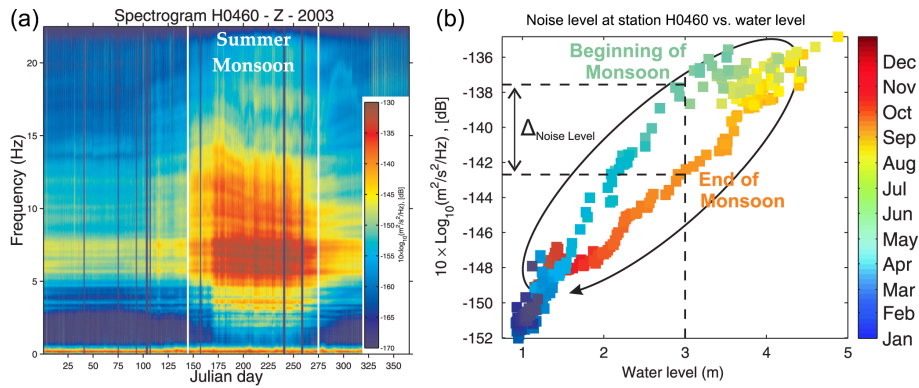


**Figure 5.** (a) Time–frequency analysis of the vertical seismic signal recorded at station H0460 from the Hi-CLIMB experiment in Nepal. Red and blue colours represent high and low level of seismic energy given in decibels relative to the velocity. (b) Daily average seismic energy in the [3–15] Hz frequency band at H0460 (a) as a function of the daily measured water level of the Trisuli River. Each square stands for a day and the colour the time evolution during 2003. After Burtin et al. (2008).

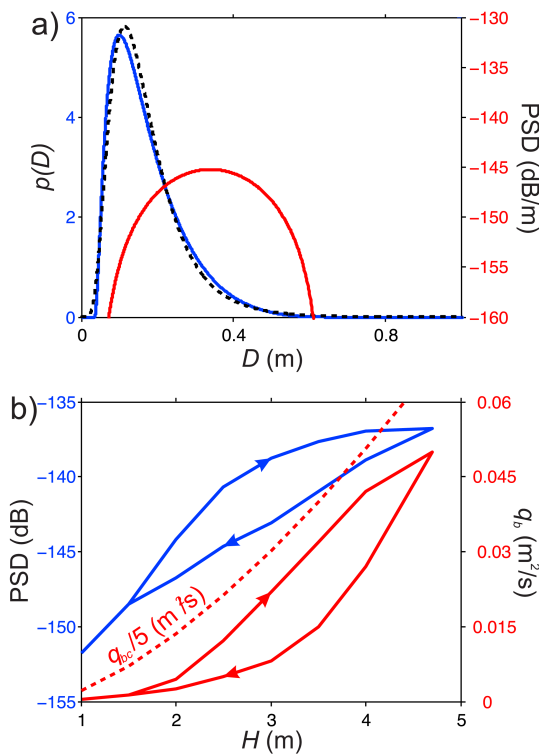


**Figure 6.** Sensitivity of power spectral density (PSD) to grain size, and inversion of PSD data for  $Q_b$  from Tsai et al. (2012). (a) Grain size probability distribution (blue) and resulting PSD (red). (b) Prediction of  $Q_b$  (red) from fitting PSD data of Burtin et al. (2008) for station H0460 (300 m from the river) at [3–15] Hz (blue).

an inverse approach to retrieve bedload flux and grain size distribution.

For reduced hydrodynamics and grain sizes several orders of magnitude smaller than those mobile in Nepal or Taiwan, the potential of seismic monitoring was explored in a small braided river plain in the French Alps (Burtin et al., 2011; Meunier et al., 2011). A frequency band of [2–5] Hz was found to best explain the fluctuation of water discharge (Fig. 7). Similarly, Schmandt et al. (2013) attributed the frequency band of [0.5–2] Hz to near-bed turbulence, the band of [2–15] Hz to the interaction between surface waves and air, and the band of [15–45] Hz to bedload transport. These observations indicate that, in the river seismic signal, the flowing water component can be spectrally isolated from the sediment component.

To improve the modelling of river seismic signal and the quantitative interpretation of recordings, Gimbert et al. (2014) modified the model of Tsai et al. (2012) to include a physical description of seismic noise generated by turbulent flow in rivers. They proposed a model focused on the generation of seismic waves from frictional forces at the riverbed due to turbulent flow interacting with boundary roughness caused by coarse sediments. The authors found that noise induced by turbulent flow excites lower frequencies than noise induced by bedload, which is in agreement with the observations made in the French Alps and at the Colorado River (Burtin et al., 2011; Schmandt et al., 2013). The model also seems to be sensitive to the source–receiver distances, where stations close to (far from) the stream have a larger fraction of noise induced by bedload (turbulent flow). From this feature, the authors concluded that the hysteresis observed along the Trisuli River is largely influenced by turbulent flow below 8 Hz. However, it is important to mention that the modelling calculations were made for a station 600 m from the river, whereas the data were recorded at a distance of 300 m. Model results of Gimbert et al. (2014) indicate that for a correct river-station distance of 300 m, bedload-induced noise should dominate the turbulent flow source. Therefore, the

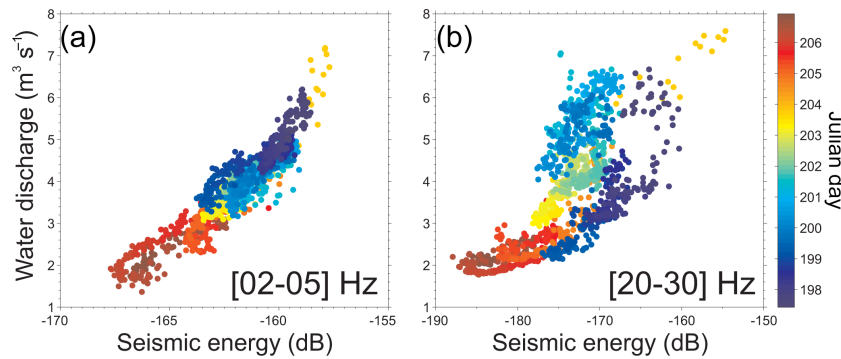


**Figure 7.** Comparison of the water discharge of the “torrent de St Pierre”, French Alps, as a function of the recorded seismic energy in decibels for a [2–5] Hz (a) and [20–30] Hz (b) frequency band. The [2–5] Hz frequency band best explains the discharge fluctuation, whereas the higher frequency bands lose this relation. These bands are interpreted to monitor the bedload transport and can be discriminated from the flowing water signal.

reduced hysteresis observed at lower frequencies (3–8 Hz) could also mean that the larger bedload fraction is less sensitive to a supply limitation during a monsoon season if the frequencies of generated ground vibrations are inversely proportional to the grain size of the colliding particles.

Indeed, seismic data analysis suggests that larger bedload particles excite lower seismic frequencies (Burtin et al., 2011; Barrière et al., 2015b). Similar observations were also inferred from laboratory and natural experiments as well as during debris-flow occurrences (Huang et al., 2004, 2007). The signal frequency content of a debris-flow forefront, where the large boulders accumulate, has much lower frequencies than the tail, where concentration of large particles drops. Finally, a dependence of the signal on particle size has been reported from in-stream monitoring (Etter, 1996; Rickenmann et al., 2014; Barrière et al., 2015b). This frequency–grain size dependence opens possibilities for indirect monitoring of bedload calibre and grain size distributions for example during floods (see Wyss et al., 2014). However, such an application requires a rigorous physical description of the phenomenon at the origin of this frequency dependency. A full development has not yet been described, but some mechanistic explanation can be found in the Hertz impulse theory (Johnson, 1987; McLaskey and Glaser, 2010; Thorne, 2014). Hence, large particles collide with the river bed over a large contact area and with a longer contact time, which would favour the generation of low-frequency content in the ground vibrations.

Although channel processes were first investigated using ambient monitoring approaches, they are not the only geomorphic activity that is recorded by seismic networks. Importantly, the sensitivity of seismometers to weak ground motion also allows surveying of slope processes (Deparis et al., 2008; Dammeier et al., 2011), and a wide range of other seismic sources, from anthropogenic activity (McNamara and Buland, 2004) to meteorological and environmental sources like rain and wind or agitated vegetation. Thus, seismome-

ter networks can be used to study both hillslope and channel processes, their interaction, and the attendant environmental conditions (Burtin et al., 2013, 2014). To understand what is recorded and to avoid misinterpretations, a source characterization needs to be performed. This is generally done with time–frequency analysis, which allows the discrimination of seismic sources, and is the topic of the next section.

### 3 Characterization of seismic signals

#### 3.1 Methods

The seismic amplitude of a time series can offer relevant information about a seismic signal but some important features can be masked by inputs that are not related to the event of interest. Filter processing, targeting specific frequencies, can help to isolate relevant parts of the signal. Transformation of the signal to obtain the frequency spectrum is a powerful tool to quantify the magnitude of a signal in the frequency domain. It allows a fast characterization of the signal and it can be used a posteriori to isolate a specific signal with a given filter. Nevertheless, in a frequency spectrum, the temporal information is not resolved and fluctuations of the spectrum in the time series are unknown. A common tool to characterize a seismic signal is time–frequency analysis since it allows combining both aspects as the seismic amplitude or energy is quantified in both time and frequency domains (Fig. 8).

A classic method in time–frequency analysis is the Fourier transform. The continuous seismic signal can be divided into short segments, on which a taper is applied and a fast Fourier transform (FFT) is performed on each individual segment to obtain a series of spectra. These are compiled in time to give the equivalent of a spectrogram, showing the distribution of seismic energy in time and frequency. With a taper it is possible to decrease the effect of spectral leakage due to limited window size. It avoids an artificial increase in power at neighbouring frequencies and allows for enhanced identification of the frequencies that characterize a signal.

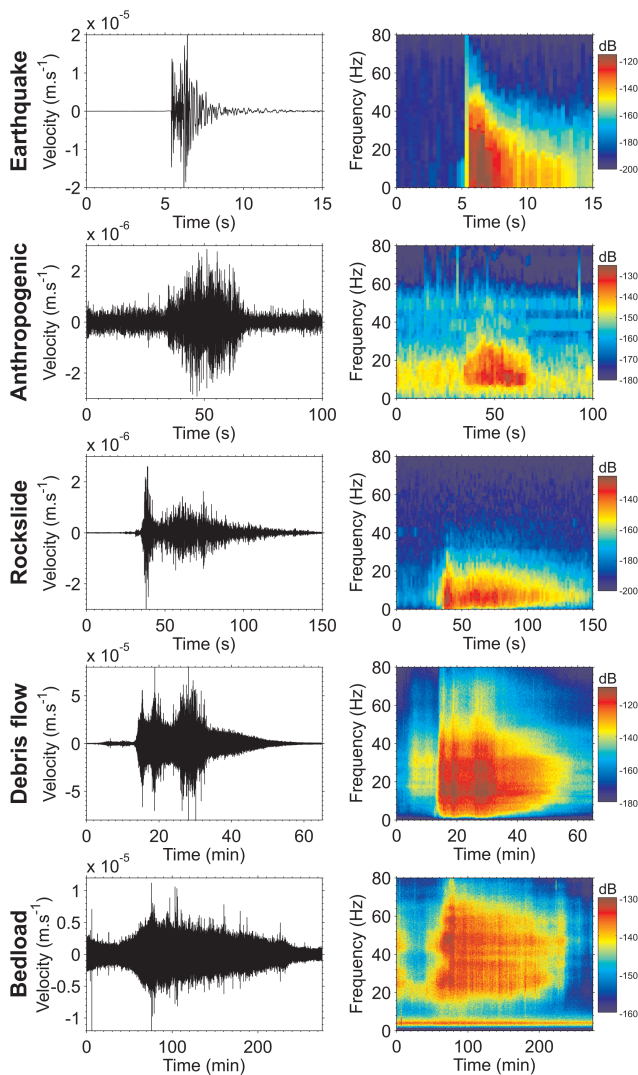


**Figure 8.** Characterization of seismic signals (left) with a time–frequency analysis (right). Each vertical seismogram is high-pass-filtered at 1 Hz and the seismic energy from spectrograms is in decibels. We performed the analysis for a local earthquake (Switzerland, day 144/2013 20:57:25 UTC), a public transport vehicle (GFZ Potsdam), a rockslide (Illgraben, day 1/2013), a debris flow (Illgraben, day 203/2013) and bedload transport (Écrins, summer 2010), from top to bottom.

To reduce the variance of the spectrum that generally arises from the simple use of a FFT and enhance the interpretation of a time–frequency analysis, several other power spectral density (PSD) estimators exist. One PSD estimator relies on Welch’s overlapping method (Welch, 1967), in which a time series is split into several overlapping segments and a PSD computed on each individual segment. Then, an average PSD over all the segments is determined, which corresponds to the PSD of the original time series. This averaging step serves to reduce the variance of the final spectrum. However, with short time series for which few data points

are processed, the splitting is a limitation since it affects the resolution of the discrete spectrum, where a limited number of frequencies are estimated. This method especially reduces the spectrum resolution at low frequencies. Thus, in a time–frequency analysis with a temporal resolution of a few seconds, Welch’s approach can be problematic for frequencies around 1 Hz. To avoid this limitation, PSDs can be computed with a multi-taper approach (Thomson, 1982; Percival and Walden, 1993). In this case, the time series is windowed with a discrete, prolate spheroidal sequence of tapers, where the taper of a given order corrects the effect of the previous order. Then, all the calculated PSDs are averaged to obtain a spectrum with a reduced variance. The advantage of a multi-taper method is that the signal is not divided, as the window size is constant, which avoids a decrease in the frequency resolution.

Time–frequency analysis is not the only approach to characterize the energy of time series. Many other methods exist for signal processing, like wavelet analysis to remove noise from the seismic records and isolate the signal of a specific process. We refer the reader to relevant review papers for details (e.g. Gröchenig, 2001; Tary et al., 2014).

### 3.2 Seismic characteristics of geomorphic sources

Time–frequency analysis of seismic signals allows the identification of seismic sources with distinct spectral signatures. We can distinguish, for example, earthquakes, rockslides, debris flows, bedload transport and anthropogenic activity (Fig. 8), based on differences between these sources in terms of the duration of a process event, the characteristic frequency range at which seismic energy is conveyed and the evolution of that frequency range over the duration of an event. Below, we review the seismic characteristics of several major geomorphic processes and other sources.

#### 3.2.1 Rockfalls, landslides and river channel processes

##### Slope processes

Among dry, gravity-driven erosion processes in steep rock walls, rockfalls, rockslides and rock avalanches tend to have a limited duration, similar to earthquakes, from several tens of seconds to a few minutes (Deparis et al., 2008; Lacroix et al., 2011; Dammeier et al., 2011; Hibert et al., 2011). However, a long rise time of seismic energy in many rockfalls contrasts with the sudden increase in energy in earthquakes. Thus, the rising time can be used to discriminate between this class of geomorphic events and earthquakes.

With frequency contents usually below 40 Hz, rockfalls tend to have complex source time functions, due to independent motion of many substantial rock particles. The example spectrogram (Fig. 8) of a rockslide recorded in the Illgraben catchment in the Swiss Alps shows the emergence of seismic energy at high frequencies, and highlights activity of two different sources. The first part of the signal lasts about

10 s and is likely related to a slope failure that is followed by a free-fall of the rock mass. The second part is interpreted to represent the rolling and tumbling of rock debris down the slope over a period of about a minute. Such characteristics are common to rockfall and rockslide activity (Deparis et al., 2008). Hibert et al. (2011) studied the seismic recordings from hundreds of rockfalls triggered at the Piton de la Fournaise volcano (Réunion Island) and were able to distinguish freely falling rocks from those that had a granular flow component.

The interpretation of the seismic signal is not only useful for event discrimination but can be used to infer the characteristics of a process. One important feature is related to the mass volume mobilized in a rockfall. Hibert et al. (2011) proposed a simple method based on the ratio of seismic to potential energy of rockfalls to estimate their volume. The resolved volumes ranged from 10 to  $10^4$  m<sup>3</sup>. Using rockslide seismic signals recorded by the Swiss Seismological Service, Dammeier et al. (2011) also defined a relationship between slide metrics and seismic features, like signal duration, peak value of ground velocity envelope, envelope energy, rise time and average ground velocity. The rock mass resolved in this study ranged from  $10^3$  to  $2 \times 10^6$  m<sup>3</sup>. Other parameters can be constrained by seismology like propagation velocity, travel distance, drop height or potential energy even with recordings at high-frequency contents (Dammeier et al., 2011; Lacroix et al., 2012). Schneider et al. (2010) analysed the seismic recordings from large rock–ice avalanches ( $> 10^6$  m<sup>3</sup>). They used the seismic data as constraints to numerically model the avalanche, allowing a continuous comparison of the model during the displacement state, rather than only at the resting state. Unsurprisingly, the parameter that best correlated with the seismic signal was the total friction work, which describes the rate of energy loss by the avalanche due to friction.

Landslides are an effective source of seismic signals and the largest mass movements are recorded at a distance of several thousand kilometres (Kanamori and Given, 1982; Brodsky et al., 2003; Ekström and Stark, 2013). This feature is due to the low- and very low-frequency content ( $< 0.1$  Hz) of their seismic signals that propagate over large distances without much attenuation compare to high-frequency signals that are more sensitive to medium scattering from small-scale heterogeneities. The recording of long-period waves (20–80 s) is a major difference to other slope events, like rockfalls and rock avalanches, which mostly produce high-frequency signals ( $> 1$  Hz). However, seismic stations close to large landslides also record high-frequency signals (Favreau et al., 2010).

The study of long-period waves allows the modelling of the seismic signal and helps to infer the dynamics and characteristics of a mass movement. The simulation generally implies the use of a point force mechanism with a rigid block sliding along a slope (Brodsky et al., 2003; Allstadt, 2013; Zhao et al., 2015). Such a simulation of seismic recordings is possible because the landslide is small in comparison to

the wavelength of seismic waves and the source–receiver distances. In addition, a detailed 3-D velocity earth model is not required and a simple homogenous velocity structure is sufficient to capture most of the signal. Furthermore, long-period waves are less affected by environmental noise, which allows the analysis of high-quality signals. Using such an approach, Moretti et al. (2012) studied an ice-rock avalanche at Mount Steller in Alaska. They successfully inverted the flow time function from simulated seismic signals. It was found that the seismic recordings were better explained by simulations including active erosion, indicating that an estimate of the volume of eroded material is possible using seismic signals. Several other studies focus on diverse types of landslides (e.g. Yamada et al., 2013; Allstadt, 2013; Ekström and Stark, 2013; Zhao et al., 2015), and the modelling of seismic recordings seems to generally be a robust approach to retrieve the dynamics and characteristics of an event. Finally, the method is not exclusively developed for events on land, and seismic signal also yields valuable data on submarine mass movements (Lin et al., 2010).

#### Channel processes

The two main channelized processes that can be monitored with seismic methods are debris flows and bedload transport. Debris flows produce an intense seismic activity that can be recorded by stream-side stations (Burtin et al., 2014). On a spectrogram, a debris flow reveals a progressive to rapid increase in seismic energy in a wide high-frequency band [1–60 Hz] (Fig. 8). This increase in seismic energy corresponds to the approach and arrival of the flow front close to the recording station. The total duration of a debris-flow seismic signal is a function of the flow activity and can last several minutes to hours. In an example from the Illgraben catchment (Fig. 8), the first part of the signal has the highest seismic energy and corresponds to the head of flow, which has the greatest mass and density and the highest concentration of decimetre-size particles (Burtin et al., 2014). The tail of the signal is characterized by a gradual decay of energy due to decreasing flow level and sediment concentration.

Seismic signals of bedload transport have characteristics comparable to those of a debris flow. Bedload motion activates the entire high-frequency band, but the lowest frequencies ( $< 5$  Hz) are only active when coarse bedload is moving (Huang et al., 2007; Burtin et al., 2011). The increase in seismic energy, as well as the duration of recorded activity, depends largely on the meteorological and hydrological conditions during the flood event (rainfall, runoff etc.). As bedload transport generates a continuous ambient seismic activity due to simultaneous motion of many sediment particles, identification of single impacts at multiple stations is generally impossible (Burtin et al., 2010).

Information from spectrograms helps to determine the main characteristics of a geomorphic event. These time–frequency features can be used a priori in an automated pro-

cess for the identification of geomorphic sources and to limit the occurrence of false alarms, crucial in the development of warning systems. This discrimination can also be performed a posteriori to evaluate the relevance of the seismic monitoring of geomorphic processes. It requires reliable distinction between geomorphic sources and other sources that intrude in the frequency range of geomorphic signals. These are mainly of tectonic, meteorological or anthropogenic nature.

### 3.2.2 Tectonic and meteorological events, and anthropogenic activity

The spectrogram of a local earthquake, an event located less than 100 km from the receiver, shows an impulsive increase in seismic energy over a broad frequency range (Fig. 8), followed by a rapid energy decay that is stronger for higher frequencies. This frequency dependency illustrates the anelastic attenuation of seismic waves (Eq. 6) that propagate in a scattering medium (Toksöz and Johnston, 1981). The sudden energy increase corresponds to the impulsive arrival of a *P* wave. The signal duration of up to tens of seconds is short but increases with the event magnitude. In the case of other tectonic events, like regional and more distant (teleseismic) earthquakes, the signal duration is longer and has an important low-frequency content (e.g. Burtin et al., 2013). Such events are recorded by regional and global seismic networks, and catalogues can be investigated to discard them from the continuous seismic signal. It is worth noting that occasionally large geomorphic events are also contained in such seismic catalogues.

Meteorological events can generate seismic signals at low and high frequencies. Wind can produce important seismic background noise at frequencies below  $3.33 \times 10^{-2}$  Hz, which correspond to wave periods exceeding 30 s, due to variations in the local atmospheric pressure field that produce an effective ground displacement and rotation (e.g. De Angelis and Bodin, 2012). Broadband seismometers are sensitive to such ground tilting motions, but short-period sensors cannot record the long-period waves generated by wind. In addition, wind can generate high-frequency seismic noise when it interacts with nearby obstacles such as vegetation or fences, which vibrate and thus induce a high-frequency disturbance. It is therefore important to deploy stations away from such sources of high-frequency signal. Raindrops can also lead to an increase in seismic noise, but this seems to be highly dependent on the local environment. During an experiment for which several seismometers were deployed in a river braid plain, Burtin et al. (2011) identified a rain signal at frequencies above 70 Hz that was present only at a station installed next to a large boulder. Stations deployed without immediate proximity to large rocks did not show this signal. Raindrops falling on soft ground or soil might not be effective sources of seismic noise, in contrast to drops hitting a rock surface, where there is less scattering and a possible better coupling to

propagate seismic waves. This interpretation has to be further investigated with dedicated experiments, but the observations seem to show that rain can affect very high frequencies under specific conditions. Further, lightning and thunder produce infrasound signals below 20 Hz (Scarpetta et al., 2005; Assink et al., 2008), which can be recorded by seismometers if the coupling between acoustic and seismic domains is effective (Walker et al., 2011). Nevertheless, to our knowledge, no study containing a systematic seismic survey of lightning and thunder sources has been published.

Finally, anthropogenic activity can also give rise to seismic perturbations. It can be as diverse as industrial activity, transport noise, or people walking close to a seismometer. Despite this large variability in their origin, a few time-frequency characteristics typical for anthropogenic noise can be highlighted. The intensity of anthropogenic seismic disturbance generally follows the local work patterns, resulting in distinct daily cycles. Individual perturbations often have a short duration and mainly affect the [1–20] Hz frequency band (Fig. 8). The signal amplitude of such perturbations typically is relatively low and the signal is recorded only at nearby stations. Therefore, anthropogenic signals are rarely coherent over an entire array and this criterion helps to separate human-induced signals from geomorphic sources. Nevertheless, for geomorphological purposes it is best to avoid the deployment of instruments close to high-traffic roads, industry or houses, because these sources could mask geomorphic signals in the same frequency range.

## 4 Detection and location of geomorphic processes

### 4.1 Detection

Continuous seismic monitoring over longer time periods produces a large volume of data with a substantial number of events, making comprehensive manual detection and location expensive and prone to operator subjectivity. Automated event detection is a requirement especially for real-time monitoring. In seismology, the automated detection of earthquakes by permanent seismic arrays is a common task, which is performed in real time, according to a widely applied procedure called the short-term average/long-term average (STA/LTA) approach (e.g. Havskov and Alguacil, 2006). This approach is also relevant for geomorphological applications.

The principle of the STA/LTA approach is to continuously calculate the ratio *R* of the average of the absolute seismic amplitude or energy *u* of a short time window (STA) over long (LTA) one. An algorithm makes the computation of running averages, where

$$STA_i = STA_{i-1} + \frac{|u_i| - STA_{i-1}}{N_{STA}}, \quad (10)$$

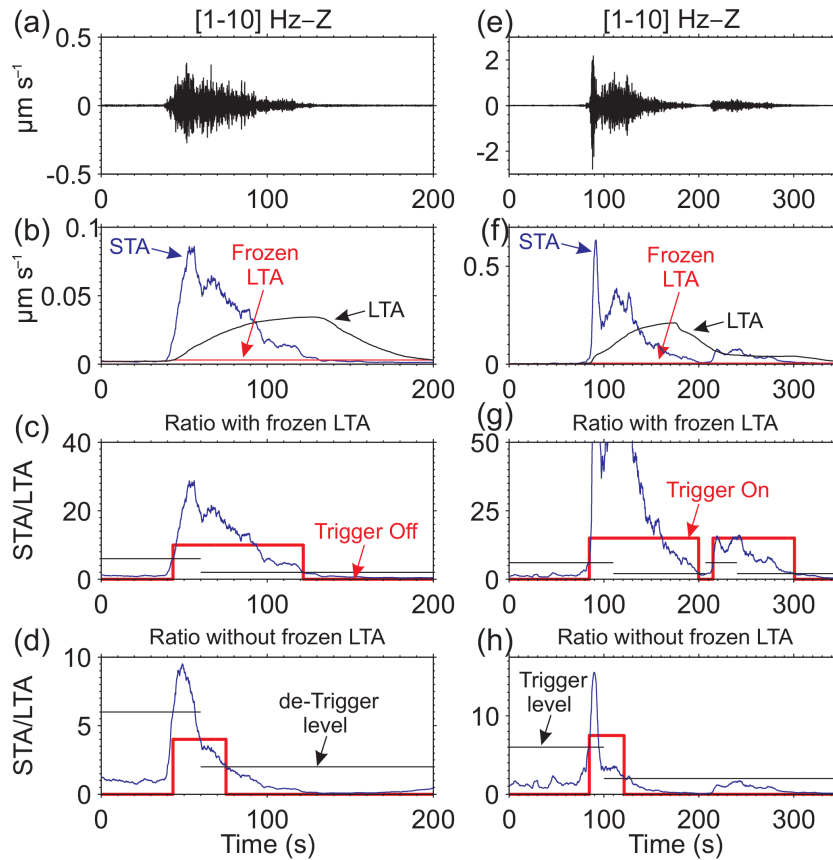


**Figure 9.** STA/LTA detection of a rockfall (left) and a rockslide (right). (a, e) [1–10] Hz band-pass-filtered recording; (b, f) STA, LTA and frozen LTA for the processed event; (c, g) STA/LTA ratio with a frozen LTA; and (d, h) STA/LTA ratio with a continuously updated LTA. The horizontal black lines represent the trigger (upper-level) and de-trigger (lower-level) threshold. The red box function illustrates the trigger state of the detection on/off (high/low).

$$LTA_i = LTA_{i-1} + \frac{|u_i| - LTA_{i-1}}{N_{LTA}}, \quad (11)$$

$$R_i = \frac{STA_i}{LTA_i}. \quad (12)$$

In these relations,  $i$  represents the sample or data point of the continuous signal and  $N_{STA}$  and  $N_{LTA}$ , the number of points taken to calculate the short and long term average, respectively. When  $R$  exceeds a pre-defined threshold, usually set from 3 to 6, a possible event is detected. If  $R$  remains above the trigger threshold over more than a given duration, the event is validated (Fig. 9). To ensure the efficiency of the STA/LTA detection, it is important to define the key parameters according to the processes to be detected. This may require training with characteristic events to increase the relevance of the algorithm and avoid false alarms or undetected events.

The STA duration is typically taken in the range from 0.5 to 5 s (e.g. Havskov and Alguacil, 2006). The shorter the duration, the more sensitive the detection is to impulsive events. For the study of geomorphic processes that have an emergent increase in seismic amplitude, the optimal STA can be quite

long, which could preclude the detection of very short events. The LTA duration should be defined to capture the fluctuation of the background seismic noise. With a long LTA,  $R$  tends to decrease rapidly, resulting in an early end of the trigger (Fig. 9d and h). Moreover, when two separate events occur in a time period less than the LTA duration, the second event may not be detected (Fig. 9h). To avoid these issues, the LTA can be frozen at the trigger value so that the ratio essentially reflects the fluctuation of STA, which is the smoothed event signal. The last parameter to define is the de-trigger threshold, which corresponds to the ratio value below which the detection of an event is terminated. The de-trigger can be equivalent to the trigger threshold but could be set to a lower value to avoid a premature end of the event detection.

To illustrate the STA/LTA approach and the utility of a frozen LTA, we show the result for two seismic records, i.e. a rockslide and a rockfall, that occurred in the Illgraben catchment, Switzerland (Fig. 9). Prior to the detection, the signal from the vertical component was filtered in the frequency band assigned to the process of interest, [1–10] Hz in this case (Fig. 9a and e). Then, the absolute value of the signal

of the vertical component was computed, but we could also have averaged the absolute amplitude from all the available components to increase the signal-to-noise ratio. The STA and LTA durations were set to 5 and 90 s, respectively. The trigger threshold was defined at  $R = 6$  and a lower value of  $R = 2$  was chosen for the de-trigger threshold. The rockfall case (Fig. 9a–d) illustrates the importance of a frozen LTA to correctly estimate the event duration: a continuously updated LTA quickly increases, whereas the STA decreases, leading to a drop of the STA/LTA before the end of the event (Fig. 9d). This does not occur with a frozen LTA (Fig. 9c). In the second seismic recording (Fig. 8e–h), the rockslide duration is evidently well estimated with a frozen LTA, but the main benefit here is in the ability to detect a second event triggered 20 s later (Fig. 9g). This event is not detected with a continuously updated LTA because the STA has a level of amplitude equivalent to the tail of LTA from the first event (Fig. 9h).

Finally, for the automatic detection of long-duration geomorphic processes, like a debris flow or a flood, the duration of the STA and the LTA has to be adapted. For this purpose, the STA should describe the duration of the seismic increase due to the flow arrival and could be set to 1–2 min. Further, the LTA should be scaled to the flow duration, from 30 to 90 min.

The detection of seismic events, including slope processes, can be performed through other methods with different levels of automation and complexities. Some methods are based on statistical properties of the time series, like the kurtosis estimate (Baillard et al., 2014; Hibert et al., 2014). The principle is to calculate the kurtosis value on running small time windows and to highlight a change the seismic amplitude distribution. Usually, background seismic noise has a normal distribution (kurtosis of 3), whereas at the onset of an event the distribution becomes non-Gaussian and the kurtosis increases rapidly (Baillard et al., 2014). This approach allows the detection of an event and the estimate of an arrival time if the amplitude onset is sufficiently impulsive. This latter can then be used in a location procedure (Baillard et al., 2014; Hibert et al., 2014).

With a more complex principle, some detection methods are based on the use of hidden Markov models. Such stochastic methods are inherited from speech recognition (e.g. Young et al., 2006) and have been successfully adapted for the detection of seismic events (e.g. Beyreuther and Wassermann, 2008; Hammer et al., 2012). With this approach an automated recognition or classification of seismic waveforms can be performed. The method can be resumed in three main stages. First, a seismic event (master event) and a sample of background seismic noise are isolated and are processed to extract features (temporal, spectral, cepstral, polarization, etc.) that well describe the class of interest. Second, the Markov model is trained to recognize the extracted features in the continuous time series according to multi-Gaussian mixture densities. Third, the algorithm is applied

to the seismic signal to compute the probabilities of likelihoods of each trained class. When a known class is detected and identified, this signal can be used to retrain the model and to increase the accuracy of the algorithm. In the case of an unclassified event, with a probability of likelihood that is too low for both seismic noise and known events, a new class is defined and the model is trained for it. Thus, the method can detect new event classes, which can thereafter be studied. The method has an interesting potential for a systematic and automated classification of geomorphic processes (Dammeier et al., 2012; Hammer et al., 2013). For a full and detailed description of the hidden Markov model approach, we refer the reader to Hammer et al. (2012, 2013).

## 4.2 Location methods

The next step is to know where in the landscape an event occurred and how it evolved both in space and time. In this analysis, the key principle relies on the observation of a coherent seismic signal at multiple stations. Then, the arrival times of the signal at the stations are used to determine the most likely location of the event, which is the origin point that best explains the observed arrival times. In this section, the location of a geomorphic process is divided into two approaches, depending on the nature of the event, either a single or short-duration event, like a rockfall, or a quasi-permanent seismic source, like bedload transport. In both cases, we need to determine an arrival time, but the procedure is different.

### 4.2.1 Discrete geomorphic events

Rockfalls, rockslides and other short-duration hillslope processes can be considered as discrete or transient events with seismic signals of up to a few minutes. If the seismic amplitude is well above the ambient noise, such an event is easily detectable with a STA/LTA approach (Sect. 4.1). For location, several strategies are then available, depending on the noise level, the signal frequency content and the seismic source type. These features affect the nature of the seismic waves that first arrive at a station. For instance, if the seismic noise level is high it may mask the first arrival, or, in the case of a slope failure, an impulsive first arrival may be recorded. Therefore, the first arrival can be an emergent or impulsive increase in seismic amplitude, making estimation of the event time at a station more, or less difficult.

For emergent signals, the most commonly employed method, called beam forming, relies on the cross-correlation of seismic records (e.g. Lacroix and Helmstetter, 2011). To determine the times of arrival  $T_i$ , the entire signal is cross-correlated, i.e. the envelope of the signal or a pre-selected time window in which a coherent wave packet is observed at many stations. In this case, the arrival time  $T_i$  at a station  $i$  is defined by

$$T_i = t_0 + l_i/V, \quad (13)$$

with  $t_0$  the origin time,  $l_i$  the distance from source to receiver and  $V$  the propagation velocity, which refers to a seismic envelope or a surface wave depending on the considered seismic signal. In a medium with a homogenous  $V$ ,  $l_i$  corresponds to the ballistic distance

$$l_i = \sqrt{(x_i - x_0)^2 + (y_i - y_0)^2 + (z_i - z_0)^2}, \quad (14)$$

where  $(x_i, y_i, z_i)$  and  $(x_0, y_0, z_0)$  are the coordinates of station  $i$  and the event, respectively. The correlation coefficient for the pair of stations  $(i, j)$  maximizes for the time delay  $dT_{i-j}$  that best corrects for the phase shift of the two signals. The time delay  $dT_{i-j}$  between stations  $i$  and  $j$  is

$$dT_{i-j} = (t_0 + l_j/V) - (t_0 + l_i/V) = (l_j - l_i)/V. \quad (15)$$

Cross-correlation allows removal of the unknown parameter  $t_0$ . Therefore, if  $V$  is unknown – which is common – then the location problem is solved by searching the location  $(x, y, z)$  and the propagation velocity  $V$  that best explains the  $dT_{i-j}$  observations.

With an array of  $N$  seismometers, a maximum of  $N(N-1)/2$  time delays can be obtained to locate the event. Then, the residuals between the observed and calculated  $dT$  are minimized. Alternatively, probability density functions can be used to map the time residuals in space (Burtin et al., 2009). Otherwise, the coherence of the cross-correlation functions can be directly mapped in the medium to retrieve the event origin (e.g. Lacroix and Helmsetter, 2011).

A separate approach relies on the polarization of the seismic waves (body waves) to estimate the direction of the incoming waves in the horizontal plane (Jurkevics, 1988). With a back projection of the arrival direction at two sites, an event can be located by triangulation, but more than two stations are required to estimate the relevance of the result. Polarization methods can only be applied if data from three-component sensors are available. However, this technique has limited potential for the study of hillslope processes because the polarization analysis is difficult to apply for high-frequency content since coherence in the signal between stations is often lost.

Finally, if the recorded event has an impulsive first arrival, like a slope failure or the impact of a freely falling object, it may be possible to identify a distinct first arrival from kurtosis-based methods (e.g. Hibert et al., 2014). Then, the location procedure is, in essence, equivalent to location technique used in the study of earthquakes with the minimization of residuals between observed and calculated arrival times or time delays (Lee and Jahr, 1972).

#### 4.2.2 Continuous geomorphic events

In contrast to hillslope processes, channel processes generate ambient seismic noise that overwhelms discrete sources (Burtin et al., 2008). This river noise is composed of sources

induced both by the flowing water and the impacts of sediment particles. A single impact isolated from other sources is easily detectable, but the same impact among thousands of others along a river reach is impossible to observe coherently at several stations. Thus, the location of sediment transport cannot be obtained from the coherent time arrivals of impacts, but another approach exists.

A location procedure for bedload transport was tested along the Trisuli River in Nepal with the data set from the Hi-CLIMB experiment (Nábělek et al., 2009; Burtin et al., 2010). The method aims to cross-correlate the continuous river seismic signals between stations, and if two receivers show coherence in the seismic signals, it means that both are recording the same sources. Thus, by locating the coherence, which consists of the space migration and the envelopes of noise correlation functions, the origin of the sources is retrieved, which is due to bedload transport in the case of river seismic signal. This approach has been previously used to locate sources of ambient seismic noise at lower frequencies ( $< 1$  Hz), such as signals from ocean swell (Shapiro et al., 2006; Rhie and Romanowicz, 2006; Gu et al., 2007). For a full description of the method, we refer the reader to Burtin et al. (2010).

Although the approach is not complex to perform, it requires some pre-processing steps that are essential to properly interpret the river seismic recordings. The continuous seismic signal is composed of ambient seismic sources, but foreign, transient events with a short duration and large amplitude, like earthquakes, landslides or human activity, can occur. When cross-correlating a 24 h long record which includes an earthquake registered at several stations, the earthquake instead of the river noise affects the cross-correlation and dominates the coherence. This effect can be avoided by applying a temporal and a frequency normalization of the raw signal. A detailed description of the necessary processing steps was given by Bensen et al. (2007), and is summarized here. The frequency normalization or spectral whitening consists of resetting the power of each frequency to an equal value, and the temporal normalization reduces the effect of short impulsive signals. Temporal normalization can be drastic using 1 bit processing, where only the sign of the time series is kept, but less drastic procedures use a running mean or clip the seismic amplitude above a given threshold. These latter approaches require some parameterization to obtain the best window length for the average or the best threshold for the clipping.

Once the continuous data are normalized, the signals are cross-correlated. If the signals are coherent, then the coherence needs to be checked for its time stability to verify that it is not induced by a single source. Time stability analysis is also required to check whether the coherence is properly associated with the processes of interest. Optimally, cross-correlation is performed at several frequencies related to sediment transport as well as other anthropogenic activity that may be continuous during the day. For the Hi-CLIMB ex-

periment (Burtin et al., 2010), only the coherence observed during the monsoon season was kept, since this time period corresponds to the highest activity of the river, both for discharge and sediment transport. The operation was performed for each available station pair along the Trisuli River and for a wide range of frequencies.

Once the library of envelope of noise correlation functions is set, time delays are converted into distances in a migration step to locate the origin of the sources. Burtin et al. (2010) found that the location of coherence along the Trisuli River was in agreement with calculated river incision rates. This similarity gives support for the strategy used to locate bedload transport. In this method, observations are made using a relative signal intensity since the normalization procedure resets the amplitude. Therefore, it is only possible to infer whether one river reach is transporting more sediment than another. However, calibration with independent measurements and the study of seismic amplitude with a noise correlation function may lead to the ability to obtain absolute transport rates.

To locate geomorphic activity, it is essential to use an array of seismometers. Arrays can have a wide range of network geometries that influence the resolution of the location and the area covered by the monitoring. Therefore, array geometry should be adapted to the specific geomorphic needs. Different types of array geometries and their advantages and disadvantages are discussed in the next section.

## 5 Array geometry

### 5.1 Linear geometry

A seismic array with a linear geometry is suitable to study channel processes, like bedload transport (Burtin et al., 2008, 2010) or the propagation of (debris) flows (Burtin et al., 2014). In the latter case, the flow velocity can be estimated from the analysis of seismic metrics. One approach consists of measuring the arrival time of the flow front at different stations, which corresponds to the time when the seismic energy exceeds the background seismic activity prior to the flow arrival. Taking into account the distances along the channel and between stations, a front velocity of the debris flow can be defined.

Other approaches can measure the velocity of the flow front. Since a seismometer is sensitive to sources that are triggered at large distances, the instrument can detect the arrival of a flow before it reaches the channel point nearest to it. Assuming that a constant seismic energy is delivered by the flow, the recorded energy should increase as the flow moves closer to the station. Indeed, the attenuation of seismic energy decays with smaller source–receiver distances. Thus, it should be possible to retrieve the front velocity from the gradient of seismic energy arrival: the larger the rate of increase, the larger the flow velocity. However, the anelastic attenuation of the medium and the wave content (body or

surface wave) needs to be taken into account, and it is not always known. Nevertheless, some measures can be taken to overcome this issue, like testing a wide range of realistic  $Q_c$  values with respect to the local lithology. An illustration of velocity estimation with this method is given in Sect. 6.2. Another complexity arises from the fact that some processes, such as debris flows, are spatially distributed seismic sources. A debris flow generates seismic noise over its entire length that can combine to modify the shape of the increase in seismic energy recorded at a station. However, large sediment particles usually concentrate in the snout of a debris flow (Iverson et al., 1997), and they can be assumed to produce larger seismic sources than the tail end of the flow (cf. Turowski et al., 2015). Thus, the method of velocity estimation described above should at least give results that are correct to first order.

The flow velocity can also be inferred from the timing of the peak energy recorded at consecutive stations. This seismic metric may exhibit some discrepancies from one site to another and may not correspond to the real flow velocity. The channel morphology influences the dynamics of a flow, leading to erosion, transport or deposition of material; pulsing transport; or spatially variable flow velocities. As a consequence, a peak of seismic energy may be uncorrelated from one station to another. To better estimate velocity, the envelope of the seismic pulses can be cross-correlated to determine the most likely time delays for the passage of a flow event at several stations. In that case, the velocity is estimated by considering the entire flow signal. The study of seismic envelopes along the channel is also interesting for the continuous characterization of a flow event. For example, the observation of a decrease/increase in seismic energy in a channel reach can be linked to the deposition or uptake of sediment particles (see Sect. 6.2).

A linear array geometry is not suitable for the monitoring of all geomorphic processes. When monitoring in-channel processes, the location of the channel is usually known and this knowledge can be used to guide the flow location process. For location of hillslope processes, the accuracy should be high in the array direction when a source is located in the same valley near the channel (Burtin et al., 2009). However, the azimuth range for all the station pairs is limited in the longitudinal direction. Therefore, a source triggered perpendicularly is not imaged well and the location process can have an ambiguous outcome. As a consequence, a linear array is best suited for the study of propagating channel processes and can be used at the scale of a watershed.

### 5.2 Small-aperture array

To better constrain the locations of spatially distributed geomorphic events, a second dimension has to be introduced into the array geometry. With a two-dimensional (2-D) array and homogeneously distributed sites, the azimuths of all the station pairs sample the entire range of fluctuations (0–

360°). As a consequence, accurate event location should be possible.

Small-aperture arrays are a type of 2-D array that consists of several seismometers deployed in rings with a maximum aperture of 0.25–1 km. The advantage of using small distances between sensors is that coherent wave packets can be observed across the entire array even for high-frequency content up to 30 Hz (Lacroix and Helmstetter, 2011; Lacroix et al., 2012), which is a key frequency band for the study of geomorphic processes. Moreover, the coherency of the seismic signals can be extracted for short time windows. Therefore, in the study of long-duration and distributed sources, like snow and rock avalanches, the propagation of the event can be tracked by locating the different wave packets. Lacroix and Helmstetter (2011) measured propagation velocities of rockfalls by tracking the different impacts along a slope. Similarly, Lacroix et al. (2012) successfully tracked the propagation of snow avalanches and estimated front velocities.

Small-aperture arrays offer many advantages for the accurate location of sources, but the location accuracy is dependent on the relative source–array distance. For distances less than 2 to 3 times the maximum array aperture, the source coordinates can be accurately retrieved. Location of more distant sources is still possible by resolving the azimuth of the incoming seismic wave front induced by the event (Almendros et al., 1999). In this case, an ambiguity in the location arises, since a direction pointing towards the source is obtained but no distance along this direction can be accurately found. To overcome this issue, one could increase the aperture of the array. However, as the distance between sensors increases, the coherency in the high-frequency seismic signals could be lost. This would result in the inability to determine the direction of the incoming seismic waves, especially from smaller sources. Therefore, the array size is a trade-off between the maximum distance at which events can be accurately located and the event size that can be observed. Small-aperture arrays are well suited for studying propagating geomorphic processes, but because of the size–distance trade-off, their use requires especially careful planning. For the surveying of geomorphic processes at a broader scale, it is necessary to operate larger arrays that surround all seismic sources of interest.

### 5.3 Local to regional 2-D array geometry

A 2-D array geometry with a large aperture (100 km) yields good constraints on the location of events within its perimeter. The setup is well suited for studying geomorphic processes distributed in a watershed or at even larger scales (Deparis et al., 2008; Lin et al., 2010; Chen et al., 2013; Burtin et al., 2013). For instance, using the permanent national seismic network of Switzerland, Dammeier et al. (2012) studied large rockslides that occurred all over the Swiss Alps in past decades. With constraints from field observations and geotechnical studies, these authors managed to define a re-

lation between seismic metrics, like the signal duration, envelope area and peak ground velocity to estimate the rock volume involved in the recorded events.

To study the finest details of geomorphic processes and the interactions amongst them, high-resolution monitoring is essential. For medium-size areas (up to  $\sim 30 \text{ km}^2$ ), this can be achieved with a limited number of stations ( $\sim 10$  instruments) and an average sensor distance of 1–5 km. Such an application is described in the following section.

## 6 Monitoring catchment dynamics

The advantages of seismic monitoring of geomorphic processes are fully revealed when it is applied to survey the geomorphic activity within an entire catchment. As an example we use some results from a campaign in the Illgraben debris-flow catchment in the Swiss Alps (Burtin et al., 2014). During the summer of 2012, an array of 10 seismometers was deployed to study the surface activity of this steep,  $10 \text{ km}^2$  catchment, which delivers 5–15 % of the sediment load of the Rhone River upstream of Lake Geneva (Schlunegger et al., 2012). The summer season usually corresponds to a period of intense erosion due to frequent convective rainstorms (Berger et al., 2011). The seismic array was designed to monitor both slope processes and channel dynamics with instruments deployed around the catchment and along the main debris-flow channel, respectively (Fig. 10a). The 2-D array had an average station spacing of 2.9 km.

### 6.1 Monitoring links between various geomorphic processes

During a moderate rainstorm with a cumulative precipitation of 18 mm, three debris flow pulses were observed downstream. During that time, the seismic array detected 15 rockfalls, located on frequently active slopes in intensely fragmented metasedimentary rocks (Bennett et al., 2013). Two of these events occurred before the initiation of the debris-flow sequence (Fig. 10). Their locations and timing during the rainstorm fit the interpretation that one of the sediment-laden flow pulses in the channel was triggered by these rockfalls. Further downstream, the debris flow erosion and/or the ground vibrations during passage of the pulse that was initiated by rockfall seem to have caused channel bank collapse. In addition to evidence from the location, this interpretation is supported by a sudden increase in seismic energy consistent with an immediate input of sediments into the flow. The observations highlight the two-way coupling between slope and river processes within a single erosion episode with a length of no more than a few tens of minutes.

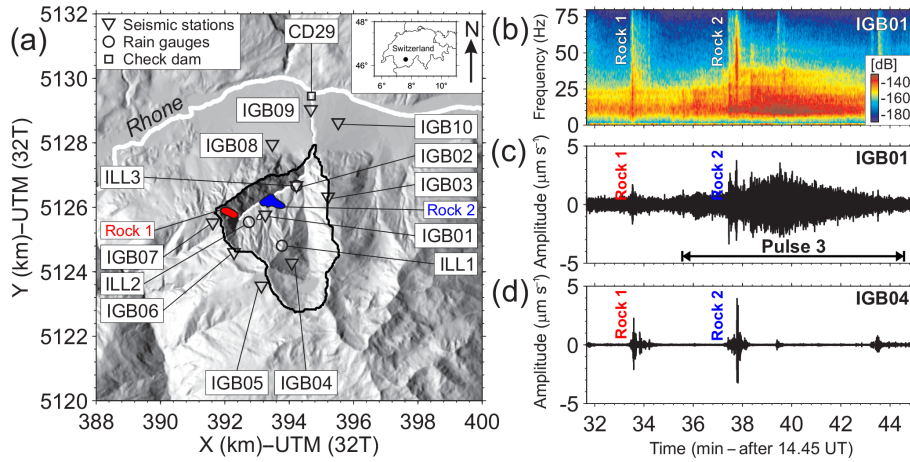


**Figure 10.** (a) The Illgraben catchment ( $\sim 10 \text{ km}^2$ , outlined in black) in Switzerland (dot in the inset map) and location of the seismological stations deployed during summer 2011 (inverse triangles, labels IGB##), meteorological stations from the Swiss Federal Institute for Forest, Snow and Landscape Research WSL (circles, labels ILL#), and Check Dam 29 (CD29, square) where the flow depth and bedload impact rates are measured. Rock 1 and 2 are the two rockfalls related with the debris-flow sequence. (b) Spectrogram in decibels of the vertical seismic signal at station IGB01 during the flow pulse 3. (c, d) Vertical [1–50] Hz bandpass-filtered seismograms at stations IGB01 (c) and IGB04 (d). The signals of both rockfalls (Rock 1 and 2) are highlighted. After Burtin et al. (2014).

## 6.2 Channel processes and dynamics

The stations deployed along the debris-flow channel were used to seismically measure some characteristics of the sediment-laden flows. The flow velocity was inferred by the arrival time of seismic pulses at each station (Burtin et al., 2014). Average velocities between two seismometers were estimated between  $3.2$  and  $3.6 \text{ m s}^{-1}$ , and the flow pulses accelerated systematically after transition from the steep but rough catchment trunk channel to the smooth bedded channel in the debris fan downstream. The estimated velocities are in the range of previously observed debris-flow velocities in the Illgraben (Badoux et al., 2009).

Flow velocity can also be estimated using simple assumptions to simulate the increase in seismic amplitude as the flow approaches a station (Fig. 11). Taking into account the anelastic attenuation (Eq. 6) and the geometrical spreading of a body wave (Eq. 2), the amplitude  $A_i$  recorded at a station  $i$  located at a distance  $R$  from a punctual source of amplitude  $S_{\text{flow}}$  is approximately

$$A_i(R) \approx \frac{S_{\text{flow}}}{R} \times \exp\left(\frac{\pi f R}{Q_c V}\right). \quad (16)$$

If surface waves are considered to propagate in the medium, we need to change the geometrical spreading, and the equation becomes

$$A_i(R) \approx \frac{S_{\text{flow}}}{\sqrt{R}} \times \exp\left(\frac{\pi f R}{Q_c V}\right). \quad (17)$$

Therefore, if  $S_{\text{flow}}$  is constant in time, when the flow propagates towards the station  $i$ , the distance  $R$  decreases and the amplitude  $A_i$  increases (Fig. 11). To properly compare the

simulated increase in seismic energy with the observed one, we need to translate the dependency in  $R$  of  $A_i$  into the time  $t$ . This step is made with the flow velocity  $V_{\text{flow}}$  according to

$$t \approx R/V_{\text{flow}}. \quad (18)$$

To retrieve a correct time series, we have to take into account the propagation time  $\tau$  of the seismic waves. Therefore, the seismic velocity  $V$  should be known or roughly assumed since the considered travel distances are reduced ( $R < 1 \text{ km}$ ) and the seismic data are smoothed over a window lasting several minutes prior to the minimization ( $0 < \tau < 2 \text{ s}$ ). The source term  $S_{\text{flow}}$  can be more complex than a punctual source propagating downstream. In the case of a debris flow we can assume that main sources (particle impacts with the largest energy) spread on a certain length along the flow. We can also define a specific distribution of this energy, where the largest amplitudes concentrate at the flow front (Fig. 10), where the largest particles are usually observed (e.g. Okuda et al., 1980; Huang et al., 2007). In this modelling approach, the remaining unknown parameters are  $V_{\text{flow}}$  and the quality factor  $Q_c$ . We can nevertheless find them while exploring a wide range of realistic values for our context of study, where  $Q_c$  is tested from 10 to 200 and  $V_{\text{flow}}$  from 1 to  $5 \text{ m s}^{-1}$ . The best-fit model parameters are found by the minimization of the error function

$$\text{Err}(V_{\text{flow}}, Q_c) = \sqrt{\sum_1^t (A(t)_i^{\text{sim}} - A(t)_i^{\text{obs}})^2}. \quad (19)$$

For this application, the seismic energy from the debris-flow sequence recorded at 5–50 Hz by station IGB09 was used (Fig. 10) (Burtin et al., 2014). Modelling took into account

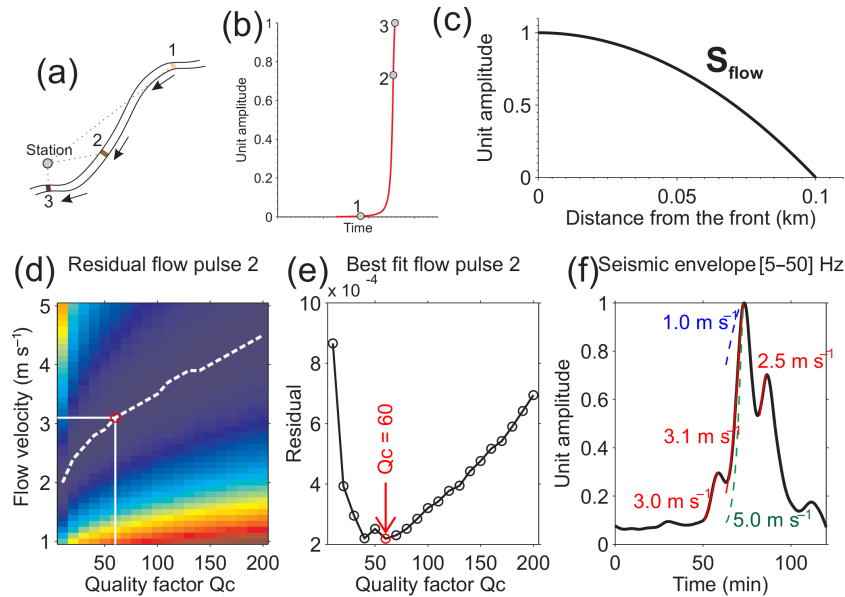


**Figure 11.** Flow pulse velocity measurement. (a) Schematic view of a flow propagating downstream. During the propagation, the flow front is getting closer to the seismic station, where the recorded seismic amplitude increases (b) due to smaller source–receiver distances. (c) Impact amplitude distribution for the debris-flow modelling. The largest sources are observed at the flow front and decrease rapidly towards the tail. (d) Residual for the velocity estimate of flow pulse 2 at IGB09 mapped in a quality factor ( $Q_c$ )–flow velocity domain. The most likely parameters that explain the recorded seismic signal are found by minimizing the residual (see Eq. 19). The white dashed line represents the local minima for each tested  $Q_c$ . (e) Residual value for each  $Q_c$  highlighted along the white dashed line in (a). For flow pulse 2, the most likely  $Q_c$  is 60 and the flow velocity is  $3.1 \text{ m s}^{-1}$ . (f) Seismic envelope at [5–50] Hz (black) recorded at IGB09 during the debris-flow sequence. The seismic data are smoothed with a 5 min length window. In red and for each flow pulse, we show the best solution. To compare and for flow pulse 2, we show the pulse shape for a velocity of  $1.0 \text{ m s}^{-1}$  (blue dashed line) and  $5.0 \text{ m s}^{-1}$  (green dashed line).

the attenuation of both body and surface waves due to geometrical spreading and the anelastic attenuation. Using this approach, the front velocities of the three flow pulses were estimated at 3.0, 3.1 and  $2.5 \text{ m s}^{-1}$ , respectively (Fig. 11). These values are comparable to, but slightly lower than, the average velocities between IGB02 and IGB09 of 3.6, 3.2, and  $3.4 \text{ m s}^{-1}$ , respectively, although comparison of the two results suggests that the last flow pulse may have slowed when approaching station IGB09 (Burtin et al., 2014).

The spatial fluctuation of the seismic energy can be used to infer channel dynamics since an increase/decrease in seismic energy is related to an increase/decrease in sediment mobility or particle impact energy (Burtin et al., 2014). Thus, the variation of seismic energy can be linked with uptake or deposition of sediments along the stream. In the Illgraben, the different flow pulses of the debris-flow sequence showed similar behaviour; in each of the three pulses, seismic energy increased inside the catchment, implying addition of sediment by bed erosion and/or lateral input. Beyond the catchment outlet, the seismic energy stayed constant or decreased slightly in the two larger flows, indicating preservation of their sediment load. In contrast, for the least energetic flow, seismic energy decreased, indicating deposition or a reduction in the concentration of large sediment particles. The latter interpretation was supported by the spectral content of the

seismic signal observed at a check dam, where bedload impact rates were also recorded. This impact record indicated a relative lack of bedload in the flow, consistent with the absence of low-frequency content in the seismic signal (e.g. Huang et al., 2007). This observation indicates that the first flow event was a hyper-concentrated flow rather than a debris flow.

### 6.3 Interests of catchment seismic monitoring and generalization

The Illgraben experiment demonstrates the potential of seismic monitoring to capture the links between various geomorphic processes. In conventional techniques, these interactions are generally inferred a posteriori and they often remain unresolved, but seismic monitoring makes their study in real time possible. Furthermore, traditional field observations are generally made on large magnitude events, since their signature in the landscape is easily identifiable. With seismic techniques small events can be explored and their role in landscape dynamics quantified. Finally, ambient seismic monitoring can be used to study processes in locations where direct field access is difficult or dangerous.

Seismic monitoring is a valuable tool for quantification of geomorphic activity for scientific purposes, but it is also in-

teresting for implementation in warning systems. In the Illgraben, a hazardous debris flow event could be detected at its inception high up in the catchment, possibly about 15 min before it debouches into settled land. Incorporating a seismic system into a real-time warning network would therefore allow for the detection of events much earlier than with the existing in-stream warning system. Minutes thus gained can make a difference when alerting inhabitants of exposed areas. Continuous monitoring of the flow velocity and seismic energy offers the opportunity of real-time observation of geomorphic processes. This information could be used to regularly update the warning status and to direct mitigation efforts.

A dense seismic array in a limited-size catchment made it possible to observe process details in the Illgraben. To achieve similar resolution in larger catchments, a commensurately larger number of seismic sensors must be deployed. An increase in the average spacing between sensors would affect the ability to detect and study smaller geomorphic events and the precision of event location. Monitoring resolution is also affected by factors such as the seismic noise level or the medium (catchment substrate) properties. Thus, there exists a trade-off between the size/density of a seismic array and the resolution that can be achieved when mapping surface activity. The exact nature of this trade-off remains to be evaluated using different environmental and instrumental settings.

## 7 Outlook

Seismic instruments allow the continuous monitoring of distributed and varied surface processes, yielding details that are difficult to acquire with classic approaches in geomorphology. The analysis of seismic signals generated by geomorphic events makes it possible to determine what happens where and when in a landscape and to resolve this geomorphic activity on the timescale of external forcing by, for example, meteorological events. Moreover, it opens a clear window on links and feedbacks between surface processes and landscape domains, and it holds the promise of real-time detection and remote observation of hazardous events. The potential of seismic monitoring has been demonstrated for diverse types of surface activity, including bedload transport, hillslope processes, and landscape erosion from oceanic coasts to steep mountain headwaters.

All applications described above share the necessity of calibration to translate the seismic signal into a geomorphic quantity and, thereby, to go beyond qualitative observation. This calibration has, for example, been performed for some surrogate monitoring methods for bedload transport (e.g. Rickenmann et al., 2012, 2014). However, it is a painstaking task, the feasibility of which is subject to the specificities of the environment (catchment size, river hydrology, channel geometry, sediment load, etc.). In the case of bedload transport, the highest transport rates and largest mobile boulders in steep mountain rivers can, at times, exceed

the capacity of available sampling devices, making direct calibration of seismic signals over the full range of bedload particle sizes and transport rates challenging. Moreover, it is difficult to imagine the existence of a universal frequency-size relation since recorded frequencies are affected by the source–receiver distances and medium properties. Therefore, the relation between frequency content and bedload size distribution is likely site-dependent. To overcome these limitations and to quantify processes, one can resort to modelling approaches (Tsai et al., 2012; Gimbert et al., 2014). Future developments of such models will need to explore more realistic sediment transport characteristics, for example by including all modes of transport, including saltation, rolling and sliding on the river bed (cf. Turowski et al., 2015). In addition, field and laboratory tests of the model on high-quality independent data are necessary.

Another important challenge for the development of a seismic survey of bedload transport is constituted by the fact that seismic instruments are sensitive to the “noise” of the flowing water in river signals, and the frequencies affected by this disturbance seem to overlap with those from bedload transport. To obtain a correct estimate of sediment transport, it is, therefore, important to discriminate the water noise from the bedload signal. A few studies have started to explore the seismic sources of flowing water, and although it seems possible to differentiate it from bedload noise, the origin of the seismic noise is still discussed (e.g. Burtin et al., 2011; Schmandt et al., 2013, Gimbert et al., 2014).

For future developments, it is important to quantify the influence of the array density on the spatial resolution of processes. This would allow optimal tailoring of arrays to the objectives of a given study. Recent work has clearly indicated the existence of a trade-off between the average instrument spacing and the ability to detect, locate and characterize the smallest events (Burtin et al., 2013, 2014). This is an important feature to also keep in mind for the eventual development of warning systems, covering relatively large regions, for the purpose of alerting authorities to the occurrence, magnitude and location of a catastrophic landslide. In regions where regular communication means are limited or disrupted after a natural disaster, seismic monitoring could help in rapid response mitigation efforts. This remote detection application complements the interest of seismic monitoring of debris flows or other flash flood events, including lake outbursts. Event detection is made at the inception and its evolution can be tracked to update the hazard risk on nearby populated areas in real time.

We anticipate that seismic monitoring of geomorphic processes will become a standard tool in the study of landscape dynamics and for the monitoring of geomorphic hazards. The required instruments and techniques along with most of the data-processing approaches are tried and tested and routinely deployed in mainstream seismology. However, to make the methodology viable for geomorphological purposes, further work is required directed at the quantification of surface pro-

cesses and the translation of seismic signals into geomorphic observations. This will be done through calibration experiments and modelling approaches, which encompass the main features of geomorphic processes. Once this is achieved, the technique will allow the continuous and detailed mapping of the surface activity in a landscape at very high temporal resolution and specified spatial precision.

**Acknowledgements.** This manuscript was initiated at an International Workshop of Acoustic and Seismic Monitoring of Bedload and Mass Movements held in Birmensdorf, Switzerland, 4–7 September 2013. The authors would like to thank the workshop organizers, and especially Dieter Rickenmann and Johnathan B. Laronne for their persistent encouragement, and the associate editor, Damià Vericat; Fabian Walter; and the two anonymous reviewers for their comments and suggestions, which helped to improve the manuscript.

The article processing charges for this open-access publication were covered by a Research Centre of the Helmholtz Association.

Edited by: D. Vericat

## References

- Aki, K. and Richards, P. G.: *Quantitative Seismology*, 2nd ed., 700 pp., Univ. Sci., Sausalito, CA, USA, 2002.
- Allstadt, K.: Extracting source characteristics and dynamics of the August 2010 Mount Meager landslide from broadband seismograms, *J. Geophys. Res.-Earth*, 118, 1472–1490, doi:10.1002/jgrf.20110, 2013.
- Almendros, J., Ibanez, J. M., Alguacil, G., and Del Pezzo, E.: Array analysis using circular-wave-front geometry: An application to locate the nearby seismo-volcanic source, *Geophys. J. Int.*, 136, 159–170, 1999.
- Andermann, C., Crave, A., Gloaguen, R., Davy, P., and Bonnet, S.: Connecting source and transport: Suspended sediments in the Nepal Himalayas, *Earth Planet Sc. Lett.*, 351–352, 158–170, doi:10.1016/j.epsl.2012.06.059, 2012.
- Anderson, J. G. and Hough, S. E.: A model for the shape of the Fourier amplitude spectrum of acceleration at high frequencies, *B. Seismol. Soc. Am.*, 74, 1969–1993, 1984.
- Assink, J. D., Evers, L. G., Holleman, I., and Paulssen, H.: Characterization of infrasound from lightning, *Geophys. Res. Lett.*, 35, L15802, doi:10.1029/2008GL034193, 2008.
- Attal, M. and Lavé, J.: Changes of bedload characteristics along the Marsyandi River (central Nepal): Implications for understanding hillslope sediment supply, sediment load evolution along fluvial networks, and denudation in active orogenic belts, edited by: Willett, S. D., Hovius, N., Brandon, M. T., and Fisher, D., *Geol. Soc. Am. S.*, 398, 143–171, doi:10.1130/2006.2398(09), 2006.
- Badoux, A., Graf, C., Rhyner, J., Kuntner, R., and McArdeall, B. W.: A debris-flow alarm system for the Alpine Illgraben catchment: design and performance, *Nat. Hazards*, 49, 517–539, doi:10.1007/s11069-008-9303-x, 2009.
- Baillard, C., Crawford, W. C., Ballu, V., Hibert, C., and Mangeney, A.: An Automatic Kurtosis-Based P- and S-Phase Picker Designed for Local Seismic Networks, *B. Seismol. Soc. Am.*, 104, 394–409, doi:10.1785/0120120347, 2014.
- Bänziger, R. and Burch, H.: Acoustic sensors as indicators for bed load transport in a mountain torrent, in: *Hydrology in Mountainous Regions I*, edited by: Lang, H. and Musy, A., IAHS Publication no. 193. IAHS: Wallingford, UK, 207–214, 1990.
- Barrière, J., Oth, A., Hostache, R., and Krein, A.: Bedload transport monitoring using seismic observations in a low-gradient rural gravel bed stream, *Geophys. Res. Lett.*, 42, 2294–2301, doi:10.1002/2015GL063630, 2015a.
- Barrière, J., Krein, A., Oth, A., and Schenkluhn, R.: An advanced signal processing technique for deriving grain size information of bedload transport from impact plate vibration measurements, *Earth Surf. Proc. Land.*, accepted, doi:10.1002/esp.3693, 2015b.
- Barros, A. P. and Lang, T. J.: Monitoring the monsoon in the Himalayas: Observations in central Nepal, June 2001, *Mon. Weather Rev.*, 131, 1408–1427, 2003.
- Bennett, G. L., Molnar, P., McArdeall, B. W., Schlunegger, F., and Burlando, P.: Patterns and controls of sediment production, transfer and yield in the Illgraben, *Geomorphology*, 188, 68–82, doi:10.1016/j.geomorph.2012.11.029, 2013.
- Bensen, G. D., Ritzwoller, M. H., Barmin, M. P., Levshin, A. L., Lin, F., Moschetti, M. P., Shapiro, N. M., and Yang, Y.: Processing seismic ambient noise data to obtain reliable broad-band surface wave dispersion measurements, *Geophys. J. Int.*, 169, 1239–1260, 2007.
- Berger, C., McArdeall, B. W., and Schlunegger, F.: Direct measurement of channel erosion by debris flows, Illgraben, Switzerland, *J. Geophys. Res.*, 116, F01002, doi:10.1029/2010JF001722, 2011.
- Berti, M., Genevois R., LaHusen R., Simoni A., and Tecca P. R.: Debris flow monitoring in the Acquabona watershed (Dolomites, Italian Alps), *Phys. Chem. Earth Pt. B*, 25, 707–715, 2000.
- Beyreuther, M. and Wassermann, J.: Continuous earthquake detection and classification using discrete Hidden Markov Models, *Geophys. J. Int.*, 175, 1055–1066, doi:10.1111/j.1365-246X.2008.03921.x, 2008.
- Bessason, B., Eiriksson, G., Thorarinnsson, O., Thorarinnsson, A., and Einarsson, S.: Automatic detection of avalanches and debris flows by seismic methods, *J. Glaciol.*, 53, 461–472, 2007.
- Brodsky, E. E., Gordeev, E., and Kanamori, H.: Landslide basal friction as measured by seismic waves, *Geophys. Res. Lett.*, 30, 2236, doi:10.1029/2003GL018485, 2003.
- Burtin, A., Bollinger, L., Vergne, J., Cattin, R., and Nábělek, J. L.: Spectral analysis of seismic noise induced by rivers: A new tool to monitor spatiotemporal changes in stream hydrodynamics, *J. Geophys. Res.*, 113, B05301, doi:10.1029/2007JB005034, 2008.
- Burtin, A., Bollinger, L., Cattin, R., Vergne, J., and Nábělek, J. L.: Spatiotemporal sequence of Himalayan debris flow from analysis of high-frequency seismic noise, *J. Geophys. Res.*, 114, F04009, doi:10.1029/2008JF001198, 2009.
- Burtin, A., Vergne, J., Rivera, L., and Dubernet, P.-P.: Location of river induced seismic signal from noise correlation functions. *Geophys. J. Int.*, 182, 1161–1173, doi:10.1111/j.1365-246X.2010.04701.x, 2010.
- Burtin, A., Cattin, R., Bollinger, L., Vergne, J., Steer, P., Robert, A., Findling, N., and Tiberi, C.: Towards the hydrologic and bed load

- monitoring from high-frequency seismic noise in a braided river: the “torrent de St Pierre”, French Alps, *J. Hydrol.*, 408, 43–53, doi:10.1016/j.jhydrol.2011.07.014, 2011.
- Burtin, A., Hovius, N., Milodowski, D. T., Chen, Y.-G., Wu, Y.-M., Lin, C.-W., Chen, H., Emberson, R., and Leu, P.-L.: Continuous catchment-scale monitoring of geomorphic processes with a 2-D seismological array, *J. Geophys. Res.-Earth*, 118, 1956–1974, doi:10.1002/jgrf.20137, 2013.
- Burtin, A., Hovius, N., McArdell, B. W., Turowski, J. M., and Vergne, J.: Seismic constraints on dynamic links between geomorphic processes and routing of sediment in a steep mountain catchment, *Earth Surf. Dynam.*, 2, 21–33, doi:10.5194/esurf-2-21-2014, 2014.
- Chao, W. A., Wu, Y. M., Zhao, L., Tsai, V. C., and Chen, C. H.: Seismologically determined bedload flux during the typhoon season, *Sci. Rep.*, 5, 8261, doi:10.1038/srep08261, 2015.
- Chen, C.-H., Chao, W.-A., Wu, Y.-M., Zhao, L., Chen, Y.-G., Ho, W.-Y., Lin, T.-L., Kuo, K.-H., and Chang, J.-M.: A seismological study of landquakes using a real-time broad-band seismic network, *Geophys. J. Int.*, 194, 885–898, doi:10.1093/gji/ggt121, 2013.
- Comiti, F., Marchi, L., Macconi, P., Arattano, M., Bertoldi, G., Borga, M., Brardinoni, F., Cavalli, M., D’Agostino, V., Penna, D., and Theule, J.: A new monitoring station for debris flows in the European Alps: first observations in the Gadria basin, *Nat. Hazards*, 73, 1175–1198, doi:10.1007/s11069-014-1088-5, 2014.
- Cook, K. L., Turowski, J. M., and Hovius, N.: A demonstration of the importance of bedload transport for fluvial bedrock erosion and knickpoint propagation, *Earth Surf. Proc. Land.*, 38, 683–695, doi:10.1002/esp.3313, 2013.
- Dammeier, F., Moore, J. R., Haslinger, F., and Loew, S.: Characterization of alpine rockslides using statistical analysis of seismic signals, *J. Geophys. Res.*, 116, F04024, doi:10.1029/2011JF002037, 2011.
- De Angelis, S. and Bodin, P.: Watching the wind; seismic data contamination at long periods due to atmospheric pressure-field-induced tilting, *B. Seismol. Soc. Am.*, 102, 1255–1265, doi:10.1785/0120110186, 2012.
- Densmore, A. L., Anderson, R. S., McAdoo, B. G., and Ellis, M. A.: Hillslope evolution by bedrock landslides, *Science*, 275, 369–372, doi:10.1126/science.275.5298.369, 1997.
- Deparis, J., Jongmans, D., Cotton, F., Baillet, L., Thouvenot, F., and Hantz, D.: Analysis of rock-fall and rock-fall avalanche seismograms in the French Alps. *B. Seismol. Soc. Am.*, 98, 1781–1796, doi:10.1785/0120070082, 2008.
- Díaz, J., Ruíz, M., Crescentini, L., Amoroso, A., and Gallart, J.: Seismic monitoring of an Alpine mountain river, *J. Geophys. Res. Sol.-Ea.*, 119, 3276–3289, doi:10.1002/2014JB010955, 2014.
- Ekström, G. and Stark, C. P.: Simple scaling of catastrophic landslide dynamics, *Science*, 339, 1416–1419, doi:10.1126/science.1232887, 2013.
- Erickson, D., McNamara, D. E., and Benz, H. M.: Frequency-dependent  $L_g$  Q within the continental United States, *B. Seismol. Soc. Am.*, 94, 1630–1643, 2004.
- Etter, M.: Zur Erfassung des Geschiebetransportes mit Hydrophonen, Diploma Thesis, University of Berne and Swiss Federal Research Institute WSL, Birmensdorf, Switzerland, 110 pp., 1996.
- Favreau, P., Mangeney, A., Lucas, A., Crosta, G., and Bouchut, F.: Numerical modeling of landquakes, *Geophys. Res. Lett.*, 37, L15305, doi:10.1029/2010GL043512, 2010.
- Gabet, E. J., Burbank, D. W., Pratt-Sitaula, B., Putkonen, J., and Bookhagen, B.: Modern erosion rates in the High Himalayas of Nepal, *Earth Planet. Sc. Lett.*, 267, 482–494, doi:10.1016/j.epsl.2007.11.059, 2008.
- Gimbert, F., Tsai, V. C., and Lamb, M. P.: A physical model for seismic noise generation by turbulent flow in rivers, *J. Geophys. Res.-Earth*, 119, 2209–2238, doi:10.1002/2014JF003201, 2014.
- Govi, M., Maraga, F., and Moia, F.: Seismic detectors for continuous bed load monitoring in a gravel stream, *Hydrolog. Sci. J.* 38, 123–132, 1993.
- Gray, J. R., Laronne, J. B., and Marr, J. D. G.: Bedload-surrogate Monitoring Technologies, US Geological Survey Scientific Investigations Report 2010-5091, US Geological Survey: Reston, VA, USA, 2010.
- Gröchenig, K.: Foundations of Time-Frequency Analysis, Birkhäuser, Boston, USA, 359 pp., 2001.
- Gu, Y. J., Dublanko, C., Lerner-Lam, A., Brzak, K., and Steckler, M.: Probing the sources of ambient seismic noise near the coasts of southern Italy, *Geophys. Res. Lett.*, 34, L22315, doi:10.1029/2007GL031967, 2007.
- Hammer, C., Beyreuther, M., and Ohrnberger, M.: A seismic event spotting system for volcano fast response systems, *B. Seismol. Soc. Am.*, 102, 948–960, doi:10.1785/0120110167, 2012.
- Hammer, C., Ohrnberger, M., and Fäh, D.: Classifying seismic waveforms from scratch: a case study in the alpine environment, *Geophys. J. Int.*, 192, 425–439, doi:10.1093/gji/ggs036, 2013.
- Havskov, J. and Alguacil, G.: Instrumentation in earthquake seismology, *Modern Approaches in Geophysics*, 22, 360 pp., Springer, Dordrecht, the Netherlands, 2006.
- Helmstetter, A. and Garambois, S.: Seismic monitoring of Séchillienne rockslide (French Alps): Analysis of seismic signals and their correlation with rainfalls, *J. Geophys. Res.*, 115, F03016, doi:10.1029/2009JF001532, 2010.
- Hibert, C., Mangeney, A., Grandjean, G., and Shapiro, N. M.: Slope instabilities in Dolomieu crater, Réunion Island: From seismic signals to rockfall characteristics, *J. Geophys. Res.*, 116, F04032, doi:10.1029/2011JF002038, 2011.
- Hibert, C., Mangeney, A., Grandjean, G., Baillard, C., Rivet, D., Shapiro, N. M., Satriano, C., Maggi, A., Boissier, P., Ferrazzini, V., and Crawford, W.: Automated identification, location, and volume estimation of rockfalls at Piton de la Fournaise volcano, *J. Geophys. Res.-Earth*, 119, 1082–1105, doi:10.1002/2013JF002970, 2014.
- Hovius, N., Stark, C. P., Chu, H.-T., and Lin, J.-C.: Supply and Removal of Sediment in a Landslide-Dominated Mountain Belt: Central Range, Taiwan, *J. Geology*, 118, 73–89, doi:10.1086/314387, 2000.
- Hsu, L., Finnegan, N. J., and Brodsky, E. E.: A seismic signature of river bedload transport during storm events, *Geophys. Res. Lett.*, 38, L13407, doi:10.1029/2011GL047759, 2011.
- Huang, C. J., Shieh, C. L., and Yin, H. Y.: Laboratory study of the underground sound generated by debris flows, *J. Geophys. Res.*, 109, F01008, doi:10.1029/2003JF000048, 2004.
- Huang, C.-J., Yin, H.-Y., Chen, C.-Y., Yeh, C.-H., and Wang, C.-L.: Ground vibrations produced by rock motions and debris flows, *J. Geophys. Res.*, 112, F02014, doi:10.1029/2005JF000437, 2007.

- Iverson, R. M., Reid, M. E., and LaHusen, R. G.: Debris flow mobilization from landslides, *Annu. Rev. Earth Planet. Sci.*, 25, 85–138, 1997.
- Johnson, K. L.: *Contact Mechanics*, Cambridge University Press, New York, USA, 452 pp., 1987.
- Jurkevics, A.: Polarization analysis of three-component array data, *B. Seismol. Soc. Am.* 785, 1725–1743, 1988.
- Kanamori, H. and Given, J. W.: Analysis of long-period seismic waves excited by the May 18, 1980, eruption of Mount St. Helens – A terrestrial monopole?, *J. Geophys. Res.*, 87, 5422–5432, doi:10.1029/JB087iB07p05422, 1982.
- Lacroix, P. and Helmstetter, A.: Location of seismic signals associated with microearthquakes and rockfalls on the Séchilienne landslide, French Alps, *B. Seismol. Soc. Am.* 101, 341–353, doi:10.1785/0120100110, 2011.
- Lacroix, P., Grasso, J.-R., Roulle, J., Giraud, G., Goetz, D., Morin, S., and Helmstetter, A.: Monitoring of snow avalanches using a seismic array: Location, speed estimation, and relationships to meteorological variables, *J. Geophys. Res.*, 117, F01034, doi:10.1029/2011JF002106, 2012.
- LaHusen, R.: *Acoustic Flow Monitor System – User Manual*, US Geological Survey, Open-File Report 02-429, 16 pp., 2005.
- Lay, T. and Wallace, T. C.: *Modern Global Seismology*, Academic Press, San Diego, CA, USA, 521 pp., 1995.
- Lee, J. C. and Jahr, W. H. K.: HYP071: a computer program for hypocenter, magnitude and first motion pattern of local earthquakes, *US Geol. Surv. Open File Rep.*, Menlo Park, CA, USA, 100 pp., 1972.
- Lin, C. H., Kumagai, H., Ando, M., and Shin, T. C.: Detection of landslides and submarine slumps using broadband seismic networks, *Geophys. Res. Lett.*, 37, L22309, doi:10.1029/2010GL044685, 2010.
- McLaskey, G. C. and Glaser, S. D.: Hertzian impact: experimental study of the force pulse and resulting stress waves, *J. Acoust. Soc. Am.*, 128, 1087–1096, doi:10.1121/1.3466847, 2010.
- McNamara, D. E. and Buland, R. P.: Ambient noise levels in the continental United States, *B. Seismol. Soc. Am.*, 94, 1517–1527, doi:10.1785/0120030001, 2004.
- Meunier, P., Burtin, A., Houssais, M., Souloumiac, P., and Métivier, F.: Discharge and sediment Transport of a small braiding river inferred from seismic survey, *Geophysical Research Abstracts*, 13, EGU General Assembly, Abstract EGU2011–13076, Vienna, Austria, 2011.
- Mizuyama, T., Laronne, J. B., Nonaka, M., Sawada, T., Satofuka, Y., Matsuoka, M., Yamashita, S., Sako, Y., Tamaki, S., Watari, M., Yamaguchi, S., and Tsuruta, K.: Calibration of a passive acoustic bedload monitoring system in Japanese mountain rivers, in: *Bedload-surrogate Monitoring Technologies*, edited by: Gray, J. R., Laronne, J. B., and Marr, J. D. G., US Geological Survey Scientific Investigations Report 2010-5091, US Geological Survey: Reston, VA, USA, 296–318, 2010a.
- Mizuyama, T., Oda, A., Laronne, J. B., Nonaka, M., and Matsuoka, M.: Laboratory tests of a Japanese pipe geophone for continuous acoustic monitoring of coarse bedload, in: *Bedload-surrogate Monitoring Technologies*, edited by: Gray, J. R., Laronne, J. B., and Marr, J. D. G., US Geological Survey Scientific Investigations Report 2010-5091, US Geological Survey: Reston, VA, USA, 319–335, 2010b.
- Moretti, L., Mangeney, A., Capdeville, Y., Stutzmann, E., Huggel, C., Schneider, D., and Bouchut, F.: Numerical modeling of the Mount Steller landslide flow history and of the generated long period seismic waves, *Geophys. Res. Lett.*, 39, L16402, doi:10.1029/2012GL052511, 2012.
- Nábělek, J., Hetényi, G., Vergne, J., Sapkota, S., Kafle, B., Jiang, M., Su, H., Chen, J., Huang, B.-S., and the Hi-CLIMB Team: Underplating in the Himalaya-Tibet collision zone revealed by the Hi-CLIMB experiment, *Science*, 325, 1371–1374, doi:10.1126/science.1167719, 2009.
- Nakamura Y.: A method for dynamic characteristics estimation of subsurface using microtremor on the ground surface, *Quarterly Report Railway Tech. Res. Inst.*, 30, 25–30, 1989.
- Okuda, S., Okunishi, K., and Suwa, H.: Observation of debris flow at Kamikamihori Valley of Mt. Yakedade, in: *Excursion Guidebook of the Third Meeting of IGU commission on Field Experiment in Geomorphology*, Disaster Prev. Res. Inst., Kyoto Univ., Kyoto, Japan, 127–130, 1980.
- Percival, D. B. and Walden, A. T.: *Spectral Analysis for Physical Applications: Multitaper and Conventional Univariate Techniques*, Cambridge Univ. Press, Cambridge, UK, 1993.
- Rhie, J. and Romanowicz, B.: A study of the relation between ocean storms and the Earth's hum, *Geochem. Geophys. Geosy.*, 7, Q10004, doi:10.1029/2006GC001274, 2006.
- Rickenmann, D. and Fritschi, B.: Bedload transport measurements using piezoelectric impact sensors and geophones, in: *Bedload-surrogate Monitoring Technologies*, edited by: Gray, J. R., Laronne, J. B., and Marr, J. D. G., US Geological Survey Scientific Investigations Report 2010-5091, US Geological Survey: Reston, VA, USA, 407–423, 2010.
- Rickenmann, D. and McArde, B. W.: Continuous measurement of sediment transport in the Erlenbach stream using piezoelectric bedload impact sensors, *Earth Surf. Proc. Land.*, 32, 1362–1378, 2007.
- Rickenmann, D., Turowski, J. M., Fritschi, B., Klaiber, A., and Ludwig, A.: Bedload transport measurements at the Erlenbach stream with geophones and automated basket samplers, *Earth Surf. Proc. Land.*, 37, 1000–1011, doi:10.1002/esp.3225, 2012.
- Rickenmann, D., Turowski, J. M., Fritschi, B., Wyss, C., Laronne, J., Barzilai, R., Reid, I., Kreisler, A., Aigner, J., Seitz, H., and Habersack, H.: Bedload transport measurements with impact plate geophones: comparison of sensor calibration in different gravel-bed streams, *Earth Surf. Proc. Land.*, 39, 928–942, doi:10.1002/esp.3499, 2014.
- Roth, D. L., Finnegan, N. J., Brodsky, E. E., Cook, K. L., Stark, C. P., and Wang, H. W.: Migration of a coarse fluvial sediment pulse detected by hysteresis in bedload generated seismic waves, *Earth Planet. Sc. Lett.*, 404, 144–153, doi:10.1016/j.epsl.2014.07.019, 2014.
- Sanchez-Sesma, F. J., Weaver, R. L., Kawase, H., Matsushima, S., Luzon, F., and Campillo, M.: Energy partitions among elastic waves for dynamic surface loads in a semi-infinite solid, *B. Seismol. Soc. Am.*, 101, 1704–1709, 2011.
- Scarpetta, S., Giudicepietro, F., Ezin, E. C., Petrosino, S., Del Pezzo, E., Martini, M., and Marinaro, M.: Automatic classification of seismic signal at Mt. Vesuvius Volcano, Italy, using neural networks, *B. Seismol. Soc. Am.*, 95, 185–196, doi:10.1785/0120030075, 2005.

- Schlunegger, F., Norton, K., and Caduff, R.: Hillslope processes in temperate environments, in: *Treatise in Geomorphology 3*, edited by: Marston, R. and Stoffel, M., Mountain and Hillslope Geomorphology, Elsevier, London, UK, 337–354, 2012.
- Schmandt, B., Aster, R. C., Scherler, D., Tsai, V. C., and Karlstrom, K.: Multiple fluvial processes detected by riverside seismic and infrasound monitoring of a controlled flood in the Grand Canyon, *Geophys. Res. Lett.*, 40, 4858–4863, doi:10.1002/grl.50953, 2013.
- Schneider, D., Bartelt, P., Caplan-Auerbach, J., Christen, M., Huggel, C., and McArdell, B. W.: Insights into rock-ice avalanche dynamics by combined analysis of seismic recordings and a numerical avalanche model. *J. Geophys. Res.*, 115, F04026, doi:10.1029/2010JF001734, 2010.
- Shapiro, N. and Campillo, M.: Emergence of broadband Rayleigh waves from correlations of the ambient seismic noise, *Geophys. Res. Lett.*, 31, L07614, doi:10.1029/2004GL019491, 2004.
- Shapiro, N. M., Ritzwoller, M. H., and Bensen, G. D.: Source location of the 26 sec microseism from cross-correlations of ambient seismic noise, *Geophys. Res. Lett.*, 33, L18310, doi:10.1029/2006GL027010, 2006.
- Shearer, P.: *Introduction to seismology*, 2nd edition, Cambridge University Press, New York, USA, 412 pp., 2009.
- Sklar, L. and Dietrich, W. E.: Sediment and rock strength controls on river incision into bedrock, *Geology*, 29, 1087–1090, doi:10.1130/0091-7613(2001)029<1087:SARSCO>2.0.CO;2, 2001.
- Stein S. and Wysession, M.: *An Introduction to Seismology, Earthquakes and Earth Structure*, Blackwell Publishing, Malden, MA, USA, 512 pp., 2003.
- Struck, M., Andermann, C., Hovius, N., Korup, O., Turowski, J. M., Bista, R., Pandit, H. P., and Dahal, R. K.: Monsoonal hillslope processes determine grain-size-specific suspended sediment fluxes in a trans-Himalayan river. *Geophys. Res. Lett.*, 42, 2302–2308, doi:10.1002/2015GL063360, 2015.
- Suriñach, E., Sabot, F., Furdada, G., and Vilaplana, J.-M.: Study of seismic signals of artificially released snow avalanches for monitoring purposes, *Phys. Chem. Earth Pt. B*, 25, 721–727, doi:10.1016/S1464-1909(00)00092-7, 2000.
- Taniguchi, S., Itakura, Y., Miyamoto, K., and Kurihara, J.: A new acoustic sensor for sediment discharge measurement, in: *Erosion and Sediment Transport Monitoring Programs in River Basins*, edited by: Bogen, J., Walling, D. E., and Day, T. J., IAHS Publication No. 210. IAHS: Wallingford, UK, 135–142, 1992.
- Tary, J. B., Herrera, R. H., Han, J., and van der Baan, M.: Spectral estimation – What is new? What is next?, *Rev. Geophys.*, 52, 723–749, doi:10.1002/2014RG000461, 2014.
- Thomson, D. J.: Spectrum estimation and harmonic analysis, *Proc. IEEE*, 70, 1055–1096, 1982.
- Thorne, P. D.: An overview of underwater sound generated by interparticle collisions and its application to the measurements of coarse sediment bedload transport, *Earth Surf. Dynam.*, 2, 531–543, doi:10.5194/esurf-2-531-2014, 2014.
- Toksöz, M. N. and Johnson, D. H.: *Seismic Wave Attenuation*, Society of Exploration Geophysicists, Tulsa, OK, USA, 1981.
- Tsai, V. C. and Atiganyanun, S.: Green's functions for surface waves in a generic velocity structure, *B. Seismol. Soc. Am.*, 104, doi:10.1785/0120140121, 2014.
- Tsai, V. C., Minchew, B., Lamb, M. P., and Ampuero, J.-P.: A physical model for seismic noise generation from sediment transport in rivers, *Geophys. Res. Lett.*, 39, L02404, doi:10.1029/2011GL050255, 2012.
- Turowski, J. M., Lague, D., and Hovius, N.: Cover effect in bedrock abrasion: a new derivation and its implications for the modeling of bedrock channel morphology, *J. Geophys. Res.*, 112, F04006, doi:10.1029/2006JF000697, 2007.
- Turowski, J. M., Yager, E. M., Badoux, A., Rickenmann, D., and Molnar, P.: The impact of exceptional events on erosion, bedload transport and channel stability in a step-pool channel, *Earth Surf. Proc. Land.* 34, 1661–1673, doi:10.1002/esp.1855, 2009.
- Turowski, J. M., Böckli, M., Rickenmann, D., and Beer, A. R.: Field measurements of the energy delivered to the channel bed by moving bed load and links to bedrock erosion, *J. Geophys. Res.* 118, 2438–2450, doi:10.1002/2013JF002765, 2013.
- Turowski, J. M., Wyss, C. R., and Beer, A. R.: Grain size effects on energy delivery to the stream bed and links to bedrock erosion, *Geophys. Res. Lett.*, 42, 1775–1780, doi:10.1002/2015GL063159, 2015.
- Walker, K. T., Shelby, R., Hedlin, M. A. H., de Groot-Hedlin, C., and Vernon, F.: Western U.S. Infrasonic Catalog: Illuminating infrasonic hot spots with the USArray, *J. Geophys. Res.*, 116, B12305, doi:10.1029/2011JB008579, 2011.
- Welch, P. D.: The use of fast Fourier transform for the estimation of power spectra: A method based on time averaging over short, modified periodograms, *IEEE T. Acoust. Speech*, 15, 70–73, 1967.
- Whipple, K. X.: Bedrock Rivers and the Geomorphology of Active Orogens, *Annu. Rev. Earth. Pl. Sc.*, 32, 151–185, doi:10.1146/annurev.earth.32.101802.120356, 2004.
- Wyss, C. R., Rickenmann, D., Fritschi, B., Turowski, J. M., Weitbrecht, V., and Boes, R. M.: Bedload grain size estimation from the indirect monitoring of bedload transport with Swiss plate geophones at the Erlenbach stream, *River Flow 2014*, edited by: Schleiss, A., De Cesare, G., Franca, M. J., and Pfister, M., Taylor & Francis Group, London, UK, 1907–1912, ISBN 978-1-138-02674-2, 2014.
- Yamada, M., Kumagai, H., Matsushi, Y., and Matsuzawa, T.: Dynamic landslide processes revealed by broadband seismic records, *Geophys. Res. Lett.*, 40, 2998–3002, doi:10.1002/grl.50437, 2013.
- Young, S. J., Kershaw, D., Odell, J., Ollason, D., Valtchev, V., and Woodland, P.: *The HTK Book Version 3.4*, Cambridge University Press, Cambridge, UK 2006.
- Zhao, J., Moretti, L., Mangeney, A., Stutzmann, E., Kanamori, H., Capdeville, Y., Calder, E. S., Hibert, C., Smith, P. J., Cole, P., and LeFriant, A.: Model Space Exploration for Determining Landslide Source History from Long-Period Seismic Data, *Pure Appl. Geophys.*, 172, 389–413, doi:10.1007/s00024-014-0852-5, 2015.